



1 **Overview of the first HyMeX Special Observation Period over Croatia**

2  
3 *Branka Ivančan-Picek, Martina Tudor, Kristian Horvath, Antonio Stanešić, Stjepan Ivatek-Šahdan*  
4 Meteorological and Hydrological Service  
5 Grič 3, 1000 Zagreb, Croatia  
6

7 **Abstract**

8  
9 The HYdrological cycle in the Mediterranean EXperiment (HyMeX) is intended to improve the  
10 capabilities to predict high impact weather events. In its framework, the first Special Observation  
11 Period (SOP1), 5 September to 6 November 2012, was aimed to study heavy precipitation events  
12 and flash floods. Here we present high impact weather events over Croatia that occurred during  
13 SOP1. A particular attention is given to eight Intense Observation Periods (IOP)s during which high  
14 precipitation occurred over the eastern Adriatic and Dinaric Alps. During the entire SOP1, the  
15 operational models forecasts generally represented well medium intensity precipitation, while heavy  
16 precipitation was frequently underestimated by the ALADIN 8 km and overestimated at higher  
17 resolution (2 km). During IOP2 intensive rainfall event occurred in wider area of the city of Rijeka  
18 in the northern Adriatic. Short-range maximum rainfall totals have achieved maximum values ever  
19 recorded at Rijeka station since the beginning of measurements in 1958. The rainfall amount  
20 measured in intervals of 20, 30 and 40 minutes could be expected once in a more than thousand,  
21 few hundreds and hundred years respectively, and they belong to the extraordinarily rare events.  
22 The operational precipitation forecast using ALADIN model at 8 km grid spacing underestimated  
23 the rainfall intensity. Evaluation of numerical sensitivity experiments suggested that forecast was  
24 slightly enhanced by improving the initial conditions through variational data assimilation. The  
25 operational non-hydrostatic run at 2 km grid spacing using configuration with ALARO physics  
26 package further improved the forecast. This article highlights the need for an intensive observation  
27 period in the future over the Adriatic region, to validate the simulated mechanisms and improve  
28 numerical weather prediction via data assimilation and model improvements in description of  
29 microphysics and air-sea interaction.

30  
31 **Keywords:** HyMeX SOP1, Adriatic TA, heavy precipitation, ALADIN mesoscale model, data  
32 assimilation  
33



34

**1. Introduction**

35

36

37

38

39

40

41

42

43

44

45

46

47

48

49

50

51

52

53

54

55

56

57

58

59

60

61

62

63

64

65

66

67

68

69

Special Observing Period 1 (SOP1) of the *Hydrological cycle in the Mediterranean Experiment – HyMeX* project was performed from 5 September to 6 November 2012 (Drobinski et al., 2014). The main objective of SOP1 was improving understanding and forecasting of the processes leading to heavy rainfall and floods (Ducrocq et al., 2014). The characteristics of the Mediterranean region, a nearly closed basin surrounded by highly urbanized and complex terrain close to the coast, makes Mediterranean area prone to natural hazards related to the water cycle, including heavy precipitation and flash-flooding occurring mostly in the late summer and autumn. Daily precipitation amounts above 200 mm have been recorded during this season (e.g. Romero et al. 2000; Buzzi and Foschini 2000; Jansa et al. 2001, Ducrocq et al 2008). Within small and densely urbanized areas, intensive and stationary precipitation events can rapidly result in dangerous floods, sometimes leading to disastrous consequences (e.g. Silvestro et al., 2012; Rebora et al. 2013; Ivančan-Picek et al. 2014). This stresses the importance of such events through their impact on social and economic circumstances of local communities. Numerical weather prediction (NWP) models have made a significant progress through the development of convection permitting systems. However, the ability to predict such high-impact events remains limited because of the contribution of fine-scale processes not represented in NWP models, and their interactions with the large-scale processes, as well as limitations of the data assimilation and especially for the convective-scale data assimilation. HyMeX aims to improve our understanding of precipitating systems, especially processes responsible to their formation and maintenance, as well as to improve the ability of numerical weather prediction models in forecasting the location and intensity of heavy precipitation events in the Mediterranean.

The orography and thermal contrast of the Mediterranean basin together with approaching upper-level trough frequently induce lee cyclogenesis (e.g. Buzzi and Tibaldi, 1978; Horvath et al., 2006) and provide a trigger mechanism for a range of extreme weather phenomena, such as local downslope Bora windstorms (known as Bura in Croatia) (e.g. Grisogono and Belušić, 2009), strong winds Scirocco and Tramontana (Jurčec et al. 1996; Pandžić and Likso 2005; Jeromel et al., 2009) orographic precipitation, thunderstorms, supercells and mesoscale convective systems (Ivančan-Picek et al. 2003; Mastrangelo et al., 2011), and water-spouts (Renko et al., 2012). Heavy precipitation occurs preferentially downstream of a cyclone aloft (Doswell et al., 1998).

The seasonal distribution of heavy precipitation suggests the relevant role of the high sea surface temperature (SST) of the Mediterranean Sea during the autumn season, when the lower layer of the



70 atmosphere is loaded with water vapour. The large thermal gradient between the atmosphere and the  
71 sea favours intense heat and moisture fluxes, which are the energy source for storms (Duffourg and  
72 Ducrocq, 2013). As the sea provides a large source of moisture and heat, the steep slopes of the  
73 surrounding mountains in the vicinity of highly urbanized coastal areas of the Mediterranean are the  
74 key factors in determining the moisture convergence and the rapid uplift of moist and unstable air  
75 responsible for triggering condensation and convective instability processes (e.g. Rotunno and  
76 Ferretti, 2001; Davolio et al., 2009). The coastal mountains, however, are not the only sources of  
77 lifting. Favourable synoptic upper-level setting, frontal lifting associated with quasi-stationary  
78 frontal systems and lower tropospheric mesoscale convective lines may also induce the convective  
79 instability.

80

81 One of the key components of HyMeX is the experimental activity, which is aimed at better  
82 quantification and understanding of the water cycle in the Mediterranean with emphasis on intense  
83 events. Over the whole Mediterranean region three target areas (TA) have been proposed for  
84 Enhanced Observational Period (EOP) to provide detailed and specific observations for studying  
85 key processes of the water cycle (<http://www.hymex.org>). One of them is the Adriatic Sea and  
86 Dinaric Alps (Adriatic TA) which has been proposed for the study of heavy precipitation events and  
87 flash-floods and considerable effort from the Croatian meteorological community was put into the  
88 campaign.

89 The Adriatic Sea is a northwest–southeast elongated basin in the central Mediterranean sea,  
90 approximately 200 km wide and 1,200 km long and is almost entirely enclosed by mountains,  
91 namely the Apennines to the west and southwest, the Alps to the north and the Dinaric Alps to the  
92 east and southeast. These topographic features play a large role in the structure and evolution of the  
93 weather systems associated with heavy precipitation (e.g. Vrhovec et al., 2001; Ivančan-Picek et al.  
94 2014). This area is one of the rainiest in Europe with expected annual amounts of precipitation  
95 greater than 5.000 mm in the mountainous hinterland on the south (end) part of the Adriatic Sea  
96 (Magaš, 2002).

97

98 Although the Adriatic TA was not a part of extensive experimental activity during the SOP1, many  
99 events that affected the Western Mediterranean expanded at the Adriatic area too. During SOP1, 16  
100 IOPs were dedicated to heavy precipitation events (HPE) over France, Spain and Italy and many of  
101 these events subsequently affected the eastern Adriatic Sea and Croatia.

102

103 The aim of the paper is: 1. to provide a scientific overview of the HPEs that affected the Adriatic TA



104 during SOP1; 2. to provide and examine the operational numerical models skill of the precipitation  
105 forecasts in Croatia; 3. to provide a detailed description of the extraordinarily rare heavy  
106 precipitation event IOP2.

107

108 The remainder of this paper is organised as follows. Section 2 describes the area of Dinaric Alps  
109 and the Adriatic region, measured and model data provided by Croatian Meteorological and  
110 Hydrological Service (DHMZ). Section 3 analyses the events during HyMeX SOP1 that produced  
111 more than 100 mm of precipitation during 24 hours on eastern Adriatic coastline. Performance of  
112 the operational precipitation forecasts is assessed through verification of forecasts mostly with the  
113 Croatian surface observation network. In Section 4 an additional attention is given to the  
114 extraordinarily rare heavy precipitation event IOP2.

115 Finally, we analyse and discuss the potentials for improving numerical weather predictions through  
116 data assimilation using sensitivity experiments. The summary and conclusions are reported in  
117 Section 5.

118

## 119 **2. HyMeX SOP1 in Croatia: observations and models**

120

121 Mediterranean is one of the climatically most pleasant areas in the world. Nevertheless, the area is  
122 prone to high-impact weather phenomena, affecting people's lives and activities and causing  
123 extensive material damage. This context was favourable for an active participation of the Croatian  
124 scientific community in the HyMeX project. Croatian research community was active in the  
125 preparation of the scientific programme included the identification of typical weather patterns over  
126 the regions and the target areas. During the SOP1, the national meteorological service supported the  
127 main HyMeX Operational Centre (HOC) in Montpellier (France), through visiting scientists and  
128 their meteorological expertise as well as providing observations, numerical modelling products and  
129 forecast data.

130

131 This section summarizes the observational network in Croatia operational during SOP1 and the  
132 operational forecasting modelling chain producing numerical weather predictions during SOP1.

133

134

### 135 **2.1. Observations**

136

137 The instrumentation deployed over the Adriatic TA during the SOP1 belongs mainly to the  
138 observational network of DHMZ. DHMZ deployed a ground observation operational network that



139 includes automatic, climatological and raingauge stations, two radio-soundings (Zagreb-Maksimir  
140 (station ID = 14240, H = 123 m asl,  $\varphi = 45^{\circ}49'N$ ,  $\lambda = 16^{\circ}02'E$ ) and Zadar-Zemunik (station ID =  
141 14430, H = 88 m asl,  $\varphi = 44^{\circ}5'N$ ,  $\lambda = 15^{\circ}21'E$ )) and two radars (Bilogora and Osijek).

142

143 The meteorological measurements and observations on 58 SYNOP stations are done every hour and  
144 reported in real time during the SOP1. Majority of SYNOP stations are also equipped with an  
145 automatic station. All automatic stations measure data with a 10 minute interval and report the  
146 measured data in real time. However, not all 63 automatic stations measure all the meteorological  
147 parameters. There are 21 automatic stations that report only the wind parameters (average 10  
148 minute speed and direction, wind gust speed measured in the last 10 minutes). Five more stations  
149 measure the wind parameters, temperature and relative humidity. All real time surface measurement  
150 (SYNOP, and automatic station data), and available radar figures are stored in HyMeX data centre.

151

152 The dense network of climatological stations is the source of temperature, humidity and wind speed,  
153 cloudiness and visibility are estimated by observation only 3 times a day at 0600, 1300 and 2000  
154 UTC; accumulated rainfall and snow height are measured at 0600 UTC (there were more than 500  
155 stations reporting accumulated 24-hourly rainfall).

156

157 In addition to operational radio-sounding in Zadar-Zemunik at 0000 and 1200 UTC several extra  
158 radiosoundings were deployed through Data Targeting System (DTS) upon request of the HOC.  
159 These targeted radiosoundings, among others in the western Mediterranean, were activated during  
160 IOP16, which caused heavy precipitation, strong winds and snow in the eastern Adriatic. The  
161 requests for additional radiosoundings at 0600 and 1800 UTC were carried out under the  
162 EUMETNET Observation Programme. Sounding data measured at Zadar-Zemunik, located on the  
163 eastern coast of the Adriatic Sea at the southern end of Velebit Mountain, provided information on  
164 the vertical structure of the troposphere in order to monitor the upstream flow of the precipitation  
165 events in the Adriatic region. The selection of sensitive area predictions (SAP) used methods  
166 developed by ECMWF and Meteo-France (Prates et al., 2009). The verification area selected for  
167 SAP calculations was centred over the northern and/or central Adriatic.

168

169 To complement the ground-based observations, the data from two radars in Croatia (Bilogora  
170 (H=270 m asl,  $\varphi = 44^{\circ}53'N$ ,  $\lambda = 17^{\circ}12'E$ ) and Osijek (H=89 m asl,  $\varphi = 45^{\circ}30'N$ ,  $\lambda = 18^{\circ}34'E$ )) and  
171 one in Slovenia (Lisca; H=944 m asl,  $\varphi = 46^{\circ}04'N$ ,  $\lambda = 15^{\circ}17'E$ ) are available operationally in a  
172 graphic form. The estimation of the instantaneous surface rain rate from Lisca and Bilogora radars  
173 were provided to the HyMeX web server in real time. Northwest Croatia, particularly Rijeka and



174 Istria are covered by operational radars in Croatia, Slovenia and Italy but the area is on the edge of  
175 the ranges and behind a mountain obstacle.

176

177 The standard Meteosat Second Generation (MSG) Spinning Enhanced Visible and Infrared Imager  
178 (SEVIRI) data are available with an interval of 15 minutes and Rapid Scan Service (RSS) data are  
179 available with 5 minute interval. The abundance of remote sensing data on the HyMeX server  
180 encourages detailed analyses of all the cases that produced HPEs over Croatia during SOP1.

181

182 Satellite derived precipitation data are used as provided from the Tropical Rainfall Measuring  
183 Mission (TRMM, Huffman et al., 2007). In particular we used the 3 hourly accumulated  
184 precipitation data from the 3B42RT product to compute the 24 hourly accumulated rainfalls for the  
185 period from 0600 UTC to 0600 UTC the next day, and 1 hourly precipitation data from 3B41RT  
186 product to compare it with the precipitation forecast by operational numerical weather prediction  
187 models.

188

189

### 190 **2.3 Mesoscale models**

191

192 During the SOP1, DHMZ provided the products from the operational forecast (Tudor et al., 2013).  
193 At the time it consisted of ALADIN model (Aladin International Team, 1997; Tudor et al. 2013) run  
194 twice per day on a domain in 8 km resolution (Figure 1a) starting from 0000 and 1200 UTC  
195 analyses up to 72 hours lead time. The operational suite used lateral boundary conditions from the  
196 global model ARPEGE run operationally in Meteo-France. The initial fields are obtained using data  
197 assimilation procedure (Stanešić, 2011). The high 2 km resolution forecast (Tudor and Ivatek-  
198 Šahdan, 2010) using ALADIN model with non-hydrostatic dynamics (Benard et al 2010) with the  
199 physics package that included the convection scheme was running operationally during the HyMeX  
200 SOP1 campaign (Figure 1b). The convection scheme used in the high-resolution model is modular  
201 multiscale microphysics and transport (3MT) scheme for precipitation and clouds (Gerard and  
202 Geleyn, 2005; Gerard, 2007; Gerard et al., 2009). Both runs use SST from the initial file of the  
203 global model ARPEGE forecast.

204

205 A short description of the models characteristics and the operational set-up during SOP1 is given in  
206 the following sub-sections.

207

208

209

210



### 211 2.3.1 Operational 8 km ALADIN forecast

212

213 The operational ALADIN model is a limited-area model that applies Fourier spectral representation  
214 of the model variables using fast Fourier transforms (FFTs) in both directions with a quadratic  
215 elliptic truncation (Machenhauer and Haugen, 1987) that ensures an isotropic horizontal resolution  
216 and that the nonlinear terms of the model equations are computed without aliasing. The forecast in 8  
217 km resolution is run on a domain with 240x216 grid points that includes a band of 11 points along  
218 northern and eastern boundaries with unphysical terrain created for the biperiodization (Figure 1a).  
219 The dynamical computations are performed using semi-implicit semi-lagrangian discretisation  
220 (Robert, 1982) to solve the hydrostatic dynamics and finite difference method on 37 levels of hybrid  
221 pressure type eta coordinate (Simmons and Burridge, 1981) in the vertical. The operational physics  
222 package at the time used prognostic TKE, cloud water and ice, rain and snow and diagnostic  
223 scheme for deep convection. The prognostic equations for condensates are solved using the  
224 barrycentric approach (Cathy et al., 2007).

225

226 A physical horizontal diffusion scheme, called semi-Lagrangian horizontal diffusion (SLHD), is  
227 based on the physical properties of the flow (Váňa et al., 2008) consists of combining two semi-  
228 Lagrangian interpolators of different diffusivity with the flow deformation as a weighting factor.  
229 The primitive prognostic equations are solved for the prognostic variables using the stable  
230 extrapolation two time level, semi-implicit, semi-Lagrangian advection scheme (SETTLS, Hortal  
231 2002) with a second-order accurate treatment of the nonlinear residual (Gospodinov et al., 2001).

232

233 The coupling of the model variables along the lateral boundaries is done using relaxation scheme  
234 (Davies, 1976) in a zone 8 grid points wide using time dependent and periodic LBCs (Haugen and  
235 Machenhauer, 1993) at the end of the grid-point computations (Radnoti, 1995) due to constraints  
236 imposed by the model dynamics. The prognostic LBCs were operationally taken from the global  
237 model ARPEGE (while there were alternative LBCs available from IFS too). The initial conditions  
238 are computed using 3dVar for the upper air fields (Hollingsworth et al 1998; Lorenc, 1986) and  
239 optimal interpolation for surface. The operational background error matrix for 3dVar data  
240 assimilation for the ALADIN weather prediction system at DHMZ was calculated using standard  
241 NMC procedure (Parrish and Derber, 1992; Bölöni and Horvath, 2010). Observations used in the  
242 data assimilation system include ground station observations (2 metre temperature, 2 metre relative  
243 humidity, pressure), radiosoundings (temperature, humidity, wind components), aircraft-based  
244 observations (temperature, wind components), wind components derived from a cloud motion  
245 detection process based on the measurements of geostationary satellites and brightness temperature



246 coming from geostationary and polar satellites. Around ~15000 observational data per assimilation  
247 cycle remains active after observation pre-processing.

248

249 In the physics parameterization package used operationally, there is a simple microphysics scheme  
250 with prognostic cloud water and ice, rain and snow (Catry et al., 2007) combined with a statistical  
251 approach for sedimentation of precipitation (Geleyn et al., 2008). The operational radiation scheme  
252 (Ritter and Geleyn 1992) based on Geleyn and Hollingsworth (1979) and enhanced recently  
253 (Geleyn et. al. 2005a, 2005b) is simple and computationally cheap using only one spectral band for  
254 computation of the long-wave and one for short-wave radiation. The turbulence contribution is  
255 computed using prognostic TKE (turbulent kinetic energy) according to Geleyn et al. (2006),  
256 modified from Louis et al. (1982) type scheme and includes a contribution of the shallow  
257 convection (Geleyn, 1987). The exchange with surface is computed using the Interaction Soil  
258 Biosphere Atmosphere (ISBA) surface scheme (Noilhan and Planton, 1989) that is also used in the  
259 surface data assimilation (Giard and Bazile, 2000). Wind, temperature and humidity on the heights  
260 of the standard meteorological measurement (10 and 2 meters above ground) are computed by  
261 interpolation from the lowest model level (about 17 meters above ground) using a parameterised  
262 vertical profile (Geleyn, 1988) dependent on stability.

263

### 264 **2.3.2 Operational 2 km non-hydrostatic ALADIN forecast**

265

266 Upon numerous case studies of severe weather events (e.g. Tudor and Ivatek-Šahdan, 2010),  
267 additional operational forecast run was established in July 2011 that uses ALADIN with non-  
268 hydrostatic dynamics and a complete set of physics parameterisations, including the convection  
269 scheme. Most of the setup in dynamics and physics is similar to the 8 km resolution operational  
270 forecast, apart from the non-hydrostatic dynamics (Benard et al., 2010). The 8 km resolution run  
271 used operationally a diagnostic convection scheme (Geleyn et al., 1995), while the 2 km resolution  
272 run used a prognostic convection scheme (Gerard and Geleyn, 2005; Gerard, 2007) that allows  
273 combining resolved and convective contributions in the grey zone (Gerard et al., 2009). The  
274 convective scheme available for the operational forecast in 2012 did not use the complete  
275 prognostic convection scheme with prognostic entrainment, but only prognostic mesh fractions and  
276 vertical velocities in updraft and downdraft. This forecast run is computed once per day, following  
277 the 0000 UTC operational 8 km resolution forecast. It uses the 6 hour forecast from the 8 km  
278 resolution operational run as input initial file and is initialized using scale selective digital filter  
279 initialization (SSDFI, Termonia 2008). Hourly 8 km forecast interpolated to 2 km resolution are  
280 used as LBC (lateral boundary conditions) files. The forecast range is 24 hours, until 0600 UTC on



281 the next day that allows comparison to precipitation data from the rain-gauges available in the high  
282 resolution network. Taking into account limitation due to computer resources and time constraints  
283 of forecast availability this setup was made in order to provide as soon as possible high resolution  
284 forecast for current day. Future upgrades will include longer time range of forecast and initialization  
285 by implementing data assimilation procedure. While other approaches such as data assimilation  
286 cycle at 2 km grid spacing, or initiation of the 2 km model with 8 km analysis at 0006 UTC may be  
287 more favourable, the described set-up is designed to mitigate the insufficient computing resources  
288 available.

289

290

### 291 **3. Heavy precipitation events over the Adriatic TA during SOP1**

292

293 In late summer and early autumn 2012 (from 5 September to 6 November), Hymex SOP1 which  
294 was dedicated to heavy precipitation and flash floods took place over the western Mediterranean  
295 (Ducrocq et al, 2014). During SOP1 20 IOPs were declared and 8 of these events affected the  
296 Adriatic TA (Table 1). Most of these events (6 IOPs) were dedicated to HPEs over the northern  
297 Adriatic (city of Rijeka).

298 Figure 2a shows the total precipitation measured by the Croatian rain gauge network cumulated  
299 over the whole SOP1. The total precipitation for the SOP1 was above the corresponding  
300 climatology (Zaninović et al., 2008) for September and October for Adriatic TA. Similar was found  
301 over the Apennine peninsula (Davolio et al., 2015). Maximum of precipitation during SOP1 was  
302 recorded on the northern Adriatic (city of Rijeka) and its mountainous hinterland of Gorski Kotar  
303 (more than 1000 mm at some locations). There were 15 days with daily rainfall accumulations  
304 exceeding 100 mm at locations in the Adriatic TA (Figure 2b). There were more IOPs dedicated to  
305 HPEs over the Adriatic TA in October than in September 2012 which was also the case in the  
306 western Mediterranean (Ducrocq et al., 2014). Several of these events caused local urban flooding  
307 (Rijeka, Pula and Zadar) with considerable material damage.

308 Some of the IOPs were embedded in a synoptic setting characterized with cyclones over the western  
309 Europe and Mediterranean recognized as a favourable conditions to heavy rainfall (e.g. Dayan et al.  
310 2015). The storm tracks of these cyclones coming from the North Atlantic to Europe depend on the  
311 direction and strength of the westerly winds controlled by the relative positions of the permanent  
312 Azores High and Icelandic Low. The variation of this relative position is known as the North  
313 Atlantic Oscillation (NAO) index, taken to be positive when the difference in pressures measured at  
314 Azores and Iceland is high and related to strong westerly wind. NAO is negative when the pressure  
315 difference is low, westerlies are reduced and storm tracks are shifted towards the Mediterranean



316 increasing the frequency and intensity of rainfall there. During the first weeks of the SOP1, NAO  
317 was in a slightly positive phase and few HPEs happened before 22 September affecting only the  
318 eastern part of the basin, particularly Adriatic area and Dinaric Alps as well as the Italian target  
319 areas. After that period, the weather above North Atlantic was characterized by mostly negative  
320 NAO and long lasting hurricane Nadine (16 September to 3 October 2012). Hurricane Nadine  
321 affected the weather not only over the Azores region it traversed, but it also modified the Rossby  
322 wave breaking downstream (Pantillon et al. 2015) and possibly reduced the long term predictability  
323 over Mediterranean.

324

### 325 **3.1 Overview of IOPs over the Adriatic TA**

326

327

328 The influence of different meteorological characteristics and physical processes that produced HPE  
329 over Adriatic target area and Dinaric Alps are briefly analysed and summarized. Previous research  
330 on HPE occurrence in the wider Adriatic region (e.g. Doswell et al., 1998; Romero et al., 1998;  
331 Vrhovec et al., 2001; Kozarić and Ivančan-Picek, 2006; Horvath et al., 2006; Mastrangelo et al.,  
332 2011; Mikuš et al., 2012) highlighted *cyclonic activity* in the western Mediterranean and in the  
333 Adriatic as a triggering mechanism for a range of extreme weather phenomena including HPE.  
334 Position of cyclones that appear in the Adriatic Sea basin strongly influence the climate and weather  
335 conditions in the area (Horvath et al., 2008).

336

337 During the SOP1 several troughs entered the western Mediterranean and produced cyclogenesis  
338 over the Gulf of Genoa or over the Tyrrhenian Sea (IOP2, IOP4, IOP16, IOP18, see Figure 3).  
339 Among those events, IOP16 and IOP18 represent excellent cases for the science issues identified in  
340 HyMeX program for the western Mediterranean (convection initiation, cloud-precipitation  
341 processes, air-sea coupled processes). These situations produce favourable conditions for HPE on  
342 the southern side of the Alpine ridge including the northern Adriatic region.

343 During these events, the Adriatic TA was strongly affected by the Genoa cyclone. Figures 3d and 3e  
344 show the sea level pressure and low-level wind vectors at 1200 UTC on 27 and 31 October. The  
345 low-level wind field was dominated by a low-level jet stream that carried the warm and humid  
346 Mediterranean air to the Adriatic Sea. This situation was favourable for the strong S-SE sirocco  
347 wind (IOP18) known as the *jugo* in Croatian (e.g. Jurčec et al., 1996).

348 During IOP16, targeted radio-soundings aimed at both data assimilation, case analysis and  
349 verification were deployed over the central Mediterranean area and Adriatic area. The time  
350 evolution of the vertical structure of troposphere on the eastern Adriatic coast is inferred by DTS  
351 deployed and standard radiosoundings at Zadar-Zemunik during 26-28 October (Figure 5). Gradual



352 moistening of the lower troposphere occurred during 26 October during southeasterly near-surface  
353 *jugo* wind in the Adriatic basin and southwesterly flow aloft. The air column below 500 hPa was  
354 nearly saturated and also rather moist above. On 26 October this moistening was still not associated  
355 with significant values of convective available potential energy (CAPE). On the next day, however,  
356 CAPE increased to over 1200 J/kg on 1200 UTC and over 1000 J/kg on 1800 UTC 27 October. The  
357 winds strengthened throughout the troposphere, and the highest intensity was observed in the layer  
358 between 300 and 200 hPa. Strong southwesterly shear of approximately 20m/s in the first 2 km of  
359 the troposphere was also present over this area.

360

361 Both IOPs (IOP16, IOP18) were fairly well forecast (Figure 4). The precipitation timing and the  
362 location of the maxima are reproduced quite well in the models forecasts. In less than 24 h, intense  
363 precipitation exceeding 170 mm affected the northern Adriatic area. Operational forecast of the 2  
364 km model resolution run overestimates rainfall above mountains, but it is consequently closer to the  
365 extreme amounts in the Rijeka area (Figure 4-B and Figure 4-C).

366

367 Occasionally a mesoscale cyclone associated with a potential vorticity (PV) anomaly formed over  
368 the Adriatic Sea developed (IOP4). This event was enhanced by the Bora flow over the northern  
369 Adriatic Sea and warm southerly wind on the southern Adriatic (Figure 3a). Mesoscale cyclone  
370 moved slowly south eastward inducing instability over central Adriatic Sea, with intense convective  
371 phenomena on both sides of the basin. Several rain gauges stations reached maxima of over 150 –  
372 200 mm/24h along the eastern Italian coast (Maiello et al., 2014) and more than 100 mm/24h was  
373 recorded over southeast coast of the Adriatic with the maximum over Pelješac peninsula. There are  
374 also local maxima in precipitation located above the sea that can be recognized in the precipitation  
375 estimates from the measured satellite data (Figure 6b).

376

377 Several events were characterized by frontal lifting associated with quasi-stationary *frontal systems*  
378 which help the release of convective instability (IOP9, IOP12, IOP13). This weather regime  
379 provided a favourable environment for HPE with thunderstorms over the northern Adriatic Sea  
380 where 127.4 mm/24h was recorded in the city of Rijeka in the northern Adriatic (IOP9). After 8  
381 days without HPE in the first part of October, weather patterns became favourable to HPE over the  
382 Adriatic TA with blocking and SW advection of warm and moist air. HPE occurred every day from  
383 11 to 16 October (IOP12, IOP13). Smooth troughs entering the western Mediterranean Sea were  
384 observed producing a south westerly flow over the Adriatic TA. A cold front was moving eastward  
385 supporting the advection of moist air on the low levels towards coastline. This warm and moist air  
386 ahead of the front supported intensive convective activity that formed a rain band stretching from



387 Tunisia over southern Italy to southeast Croatia and caused intensive precipitation with more than  
388 100mm/24 h mostly above open sea and several outermost islands (Mali Lošinj (H = 53 m asl,  $\varphi =$   
389  $44^{\circ}53'N$ ,  $\lambda = 14^{\circ}48'E$ ), Silba (H = 20 m asl,  $\varphi = 44^{\circ}37'N$ ,  $\lambda = 14^{\circ}7'E$ )).

390 Large-scale conditions such as found in these IOPs help to generate mesoscale and local processes  
391 which modify additionally flow regimes leading to quite different precipitation patterns.

392

393 Several events were characterised by convection over the sea followed by *orographic precipitation*  
394 (IOP2, IOP9, IOP16, IOP19). During the whole IOP19 (3-5 November 2012) south westerly  
395 advection of warm and humid air produced convection over the northern Adriatic and orographic  
396 precipitation along the Kvarner bay. Detailed synoptic situation is described in Ferretti et al. (2014)  
397 and Davolio et al. (2016). A south westerly flow over the whole region of the western  
398 Mediterranean was produced by a baroclinic wave that formed over northwest Europe to northern  
399 Africa due to weakened westerlies and low NAO. Strong southwest flow in lower troposphere  
400 ahead of the cold front supported advection of moist and warm air. More rainfall was recorded on  
401 rain gauges on the north eastern Adriatic coast. During this event 177.0 mm/24h was recorded in  
402 Klana, the hinterland of the city of Rijeka (Figure 4-D) and the precipitation was mainly orographic  
403 forced with strong southeast *jugo* (sirocco) wind (Figure 3f). Previous studies (e.g. Buzzi and  
404 Foschini, 2000; Ivančan-Picek et al., 2014; Davolio et al., 2016) show that the largest component of  
405 the mountain-range-scale precipitation appears to be due to the orographic lift of the moist and  
406 impinging low-level flow. Consequently, the vertical uplifts forced by the Dinaric Alps area were  
407 favourable for convection initiation and maintenance. Coastal mountains close to the Adriatic Sea  
408 are not the only sources of lifting. The low-level circulation over the sea frequently generates low-  
409 level convergence responsible for convective initiation (Jansa et al., 2001; Davolio et al. 2009).  
410 Mesoscale cyclone or frontal system moved slowly south eastward inducing instability over central  
411 Adriatic Sea usually is the cause of the strong low-level *convergence* between the southerly *jugo*  
412 (sirocco) and northeasterly *bora* wind. This was the case during IOP4 when more than 100mm/24h  
413 was recorded over the southeast Adriatic coast and above the open sea (Figure 6b).

414

415 The sirocco wind is the cause of a piling up of Adriatic water near the northernmost coasts that  
416 occasionally floods the city of Venice (Orlić et al., 1994). This was the case also during the IOP16  
417 and IOP18. The Venice Lagoon was hit by the “acqua alta” (high water), the warning level was  
418 exceeded twice with more than 120 mm on 27 and 28 October (Ferretti et al., 2014) and more than  
419 140 mm was measured on 1 November 2012. The cyclone during IOP16 caused the lowest pressure  
420 recorded over the Adriatic TA during the whole SOP1 (Figure 3d). Advection of the warm air  
421 combined with intensive advection of cyclonic vorticity contributed to the orographically induced



422 upward motion in the area of the northern Adriatic and the adjacent mountains, which resulted with  
423 HPE in city of Rijeka and mountainous hinterland (180 mm/24h).

424

425 In IOP4 heat loss caused by strong *bora* wind was very intensive. *Bora* was severe on northern  
426 Adriatic, exceeding 24 m/s. Strong *bora* wind brings cold and dry continental air over the warm  
427 Adriatic basin, generating intense air-sea heat exchanges and sea surface cooling (e.g. Grisogono  
428 and Belušić, 2009) during short time. The proper representation of sea surface temperature (SST) in  
429 the numerical models, especially in small and shallow basins like Adriatic Sea is necessary for  
430 improving the short-range precipitation forecasts (e.g. Davolio et al., 2015b; Stocchi and Davolio,  
431 2016; Ricchi et al., 2016). The response of heavy precipitation to a SST change is complex and  
432 mainly involves the modification of the boundary layer characteristics, flow dynamics and its  
433 interaction with the orography. In the numerical modelling the SST representation is generally  
434 unrealistic and usually keeps SST fixed at its initial value. Figure 6a shows SST measured on  
435 station Bakar close to the city of Rijeka for the whole SOP period. During IOP4 (13 – 14 September  
436 2012) the SST decreased for 10 °C on station Bakar in comparison to representation in operational  
437 model which use LBC from the global model ARPEGE. Therefore, the SST near the coast was  
438 colder than in the ALADIN model forecast affecting the ability of the forecast model to properly  
439 forecast the meteorological fields there. In addition to operational SST, control simulation is driven  
440 by SST field provided through the OSTIA analyses (Donlon et al., 2012). The daily accumulated  
441 precipitation for operational 2 km model run and the control simulation with modified colder SST  
442 from OSTIA are presented at Figure 6d and 6e. In this case, control simulation run is more realistic  
443 (see Figure 6b) and generally drier than the operational with a warmer SST. Colder SST resulted  
444 with decreasing of precipitation over the mountainous Adriatic coast.

445 IOP4 shows the needs for further improvements of the role of SST and surface (latent and sensible)  
446 heat fluxes over the Adriatic Sea, which attain large values during strong *bora* events. However a  
447 more detailed analysis of the impact of SST on precipitation is ongoing.

448

449

### 450 3.2. Verification of the precipitation forecasts during SOP1

451

452 Performance of the operational precipitation forecasts with the ALADIN model at 8 km and  
453 ALADIN model at 2km grid spacing during SOP1 was assessed by comparing forecasts with the  
454 measurements from Croatian surface observation network. Model results were compared with 24-  
455 hour accumulated precipitation measured by the rain gauges where before the calculation of  
456 verification scores results for ALADIN 2 km was upscaled to ALADIN 8 km grid to avoid double  
457 penalty. Contingency tables (Table 2 and 3) were evaluated with three categories defined according



458 to the amount of 24h accumulated precipitation and classified as dry, medium and strong. An event  
459 was defined as dry if 24 h accumulated precipitations on the rain gauge station was less or equal 0.2  
460 mm/24h. The border between the medium and strong categories was defined as the 95<sup>th</sup> percentile  
461 of measured 24h accumulated precipitation (50.42 mm/24h) during the SOP1 period, but with dry  
462 events excluded.

463 Figure 7 presents 24 hour accumulated precipitation histograms from both models and rain gauges  
464 during the whole SOP1 period and during the specific days corresponding to 8 IOPs indicated in  
465 Table 1. Measurements show that during the entire SOP1 period, large percentage of events was dry  
466 (64.7%). Value corresponding to the 95<sup>th</sup> percentile (50.4 mm) is indicated at graph and it appears as  
467 a reasonable threshold for heavy precipitation events that we want to verify. Histogram for IOP days  
468 only (8 IOP cases) as expected show that the number of dry events is reduced (18.1%) and relative  
469 frequency of events shifts towards events with higher amounts of precipitation.

470

471 While for the whole SOP1 period ALADIN 8 km model distribution is in rather good agreement  
472 with rain gauge measurements except for most intensive rain, the model distribution for the IOP  
473 days only shows that the model tends to underestimate frequency of weak and strong precipitation  
474 events while it overestimates frequency of moderate precipitation events. For ALADIN 2 km SOP1  
475 and IOP days only histograms shows similar results where the model tends to underestimate  
476 moderate precipitation while at the same time it tends to overestimate strong precipitation.  
477 Comparison of two models shows a better agreement of ALADIN 2km model with measurements  
478 especially for very weak and strong precipitation.

479 In Table 2 and 3 verification measures (Wilks, 2006) calculated from comparison of 24 hour  
480 accumulated precipitation from rain gauges and model, for the three categories and for different  
481 periods are summarized. As most of measures are Base Rate (BR) sensitive and they can be safely  
482 used only to compare two models for the same event, polychoric correlation coefficient (PCC; Juras  
483 and Pasarić, 2006) as additional measure was calculated because PCC does not depend on BR or on  
484 frequency bias (FBIAS). For both ALADIN models PCC show rather high level of association  
485 between observations and forecast for whole SOP1 while it has smaller value for only IOP days.

486 For both models smallest value of PCC is for IOP 9 where both models overestimated number of  
487 strong precipitation events, especially ALADIN 2 km which can be seen from much higher FBIAS  
488 than the one from ALADIN 8 km model. Comparing performance of two ALADIN models, it can  
489 be seen that ALADIN 2 km has higher level of association between observations and forecast for  
490 IOP13 and IOP19 compared to ALADIN 8 km. For IOP13 ALADIN 2 km is relatively more  
491 accurate in all three categories which can be seen from higher values of critical success index (CSI).

492 For IOP19 FBIAS values show that ALADIN 2 km overestimates frequency of strong precipitation



493 but at the same time it is relatively more accurate for other two categories (higher CSI). For dry  
494 category ALADIN 2km has better scores for almost all selected cases (higher CSI; FBIAS closer to  
495 1). For medium precipitation ALADIN 8 km has better scores except for IOP13 and IOP19. For  
496 strong category scores show that ALADIN 2 km tends to overestimate frequency of strong events  
497 while ALADIN 8 km tends to underestimate frequency of strong events with only exception for  
498 IOP19 where both models overestimated number of strong precipitation events (especially  
499 ALADIN 2 km).

500

501

#### 502 **4. IOP2 over north-eastern Adriatic TA**

503

504

505 Although the Adriatic TA was not a part of extensive experimental activity during the SOP 1, many  
506 events that affected the Western Mediterranean expanded at the Adriatic area too. During the IOP 2  
507 in the late evening hours of September 12 a rainy episode with very heavy rain falling over only a  
508 few hours have been recorded over the city of Rijeka at the northern coast of Kvarner Bay in the  
509 eastern Adriatic sea and its mountainous hinterland of Gorski kotar. According to the report of the  
510 Municipal Water and Sewer Company of the city of Rijeka some major city roads became rivers  
511 and streams, sewage manhole covers were discharged and massive caps flew into the air up to two  
512 meters, and then a spate of them were carried up to one hundred meters away from the shaft.

513 Ferretti et al. (2014) described IOP2 in north eastern Italy (NEI) and analysed the meteorological  
514 characteristics and synoptic situation. A shallow orographic cyclone developed in the lee side of the  
515 Alps extending from the Genoa Gulf to the northern Adriatic. Simultaneously with the Genoa  
516 cyclogenesis, a twin type of cyclone (Horvath et al., 2008) developed in the northern Adriatic  
517 (Figure 8 a,b). The Croatian coast of northern and middle Adriatic was influenced by the strong  
518 moist south-western flow on the leading side of the cyclone(s). The air was moist due to southwest  
519 advection and evaporation from the Mediterranean. Below 2 km there was strong convergence over  
520 the northern Adriatic. Due to its specific position deep in Kvarner bay which is open from the  
521 southwest and, at the same time, in the very pedestal of the Velebit mountain chain, the city of  
522 Rijeka and its surroundings have the geographic preconditions for pronounced convection with  
523 extensive precipitation in such specific synoptic conditions (e.g. Ivančan-Picek et al., 2003).

524 During the day in the late afternoon cold air irrupted along the Alpine slopes together with the  
525 passage of the cold front over NEI and north eastern Adriatic Sea resulted with intensive convective  
526 processes.

527

528



529 **4.1. Extreme value analysis of short-term precipitation maxima**

530

531 Spatial distribution of daily rainfall amounts for the IOP2 rain episode indicates that the largest  
532 amounts fall over the city of Rijeka (220 mm at the meteorological station Rijeka located 120 m  
533 above sea level), and the surrounding mainland hilly slopes and mountainous hinterland. According  
534 to the recorded rainfall data by ombrograph at the meteorological station Rijeka the more detailed  
535 insight into the temporal rainfall distribution during the short-term interval of this heavy rainfall  
536 event is possible (Figure 9). The rainfall episode that occurred during the six-hour period between 6  
537 pm and midnight, experienced its most intense part between 9 pm and 11 pm. Maximum 20, 30, 40,  
538 50, 60 and 120 minutes rainfall totals, which belong to this most intense part of the rainfall episode,  
539 have not been recorded at Rijeka station since the beginning of measurements in 1958 (Table 4).  
540 Especially intense were the rainfall intervals of 20, 30 and 40 minutes that could be expected once  
541 in a more than thousand, few hundreds and hundred years respectively and they belong to the  
542 extraordinarily rare event, computed from the period 1958 – 2011 (Patarčić et al., 2014). The  
543 maximum amounts that fall in the interval of two and four hours could be expected ones in forty  
544 and fifty years respectively.

545

546 **4.2 Observational analysis**

547

548 On 12<sup>th</sup> September 2012 a sequence of convective events hit the northeastern part of Italy and in  
549 particular the eastern part of Veneto and the plain of Friuli Venezia Giulia regions. During the day at  
550 least two events could be classified as supercells, the first one being also associated with a heavy  
551 hail fall (Manzato et al., 2015). After a few hours, a third storm system, resembling a squall-line,  
552 although of limited dimensions, swept over the area.

553 EUMETSAT was conducting its first experimental 2.5-minute rapid scan with the MSG-3 satellite,  
554 with data available from early morning until 0900 UTC of the IOP2 day. Unfortunately, the  
555 experimental rapid scan data with 2.5 minute interval taken by MSG-3 satellite (renamed to  
556 Meteosat-10) were available only until 0900 UTC 12 September 2012.

557 Nearby area of Istria and Rijeka received the first rain in the early afternoon that soon stopped  
558 before the torrential rain in the evening, between 2100 and 2300 UTC. The last one is connected to  
559 the third storm over Italy (as discussed in Manzato et al. 2015) that was an elongated storm moving  
560 along the coast of north Adriatic. Convection developed over the northern Adriatic and warm and  
561 moist advection produced intensive precipitation triggered by the orography inland.

562

563 Satellite data show formation of cumulonimbus clouds (Figure 10). This intensive rainfall band



564 reached Trieste and Slovenia according to radar figures (not presented) and merged with the rainfall  
565 band that formed above Trieste at 1800 UTC. Another rainfall band formed above Istria peninsula at  
566 1930 UTC. Intensive rainfall spread to Rijeka and remained there for several hours. During that  
567 time other rainfall bands formed and moved over Rijeka intensifying the precipitation and  
568 prolonging the period of high precipitation intensity.

569 According to hourly amounts, precipitation intensity was the highest from 2100 to 2200 UTC (85.3  
570 mm/h), with 20.6 and 51.7 mm/h in the previous and the next hour (Figure 9).

571  
572 Sounding data measured at Zadar-Zemunik, located about 150 km southsoutheast of the area where  
573 the largest rainfall was recorded, are shown to provide information on the vertical structure of the  
574 troposphere. Although the thermodynamic profile characteristics are not completely representative  
575 of the pre-convective environment over the study area, this is the only available sounding data on  
576 the eastern Adriatic. The soundings featured a low-level moist atmospheric layer from the surface to  
577 approximately 850 hPa connected with SE *jugo* wind, confirming a suitable environment for strong  
578 convective activity (not presented). Winds strengthened throughout the troposphere and the highest  
579 intensity was observed at 400 hPa.

580

### 581 **4.3. Operational model forecasts**

582

583

584 During the SOP1, DHMZ made available the operational forecast by ALADIN operational forecasts  
585 model in 8 km and non-hydrostatic 2 km horizontal resolution (Section 2.3). A comparison between  
586 two versions of ALADIN model is presented here and shows the capability in forecasting the  
587 intense convective activity in the area.

588 Short-range forecasts reproduced well the large-scale and mesoscale features responsible for the  
589 event (Figure 8). The low-level wind field is dominated by two low-level jet stream (LLJ) caused  
590 the appearance of the low-level wind convergence over the North Adriatic and associated with the  
591 main Genoa cyclone (Figure 8b). In this case the performance of the model is rather successful in  
592 comparison with ECMWF reanalysis (not presented). One SW LLJ was elongated from Italy  
593 towards the middle Adriatic that carry the warm and humid Mediterranean air to the Adriatic Sea,  
594 and another NE LLJ (*bora* wind) modified and intensified by the pressure gradient across the  
595 southern flank of the Alps (Figure 8a). This convergence was responsible for the convective  
596 triggering in the late afternoon. Although the mesoscale characteristics are correctly reproduced,  
597 the location and timing of precipitation was not so good. The intensive precipitation event was  
598 predicted by both models with precipitation close or exceeding 100 mm/24 hours inland of Rijeka  
599 (Figure 6), but the amount of precipitation was underestimated for the city of Rijeka that lies on the



600 coastline for all operational models possibly due to an absence of the cold pool that formed after the  
601 showers in the early afternoon or low level wind from northeast that started earlier than in the  
602 model forecast.

603 Operational forecast set-up of the ALADIN 2 km resolution run overestimates rainfall above  
604 mountains (at least when compared to the 3B41 products from the TRMM data server), but it is  
605 consequently closer to the extreme amounts measured in the Rijeka area (Figure 11). Although the  
606 3B41 product is an estimate of precipitation intensity that also suffers from errors, the rain over the  
607 southern Velebit Mountain was an overestimate, while it was correct for mountains inland of Rijeka.  
608 In the hours of peak precipitation intensity in Rijeka, the satellite measurement data-derived  
609 precipitation (TRMM 3B41RT product available from NASA's Giovanni web service) was also  
610 considerably lower than the one measured in-situ.

611 The high resolution non-hydrostatic operational forecast shows upward motions along the coastal  
612 mountains of Croatia and associated to the convergence line and the rain band over the sea (Figure  
613 12). The wave of the upward motion moves from the Po valley eastward and reaches Rijeka area  
614 one hour after the recorded maximum intensity in precipitations so the model might be little late  
615 behind the real weather events. There is also a permanent wave formed over southern Velebit (and  
616 several other mountains) that persist throughout the night. This wave is responsible for triggering  
617 the precipitation there and its intensity is probably overestimated. Apparently, small but tall  
618 topographic obstacles are able to trigger too much precipitation and this remains an issue to solve.

619  
620 Figure 13 presents a scatter plot of 24h accumulated precipitation from rain gauges over Croatia and  
621 forecast values from ALADIN model taken from the nearest grid points for IOP 2. ALADIN 8 km  
622 model underestimated precipitation and forecasted up to 92 mm/24h of rainfall while measurements  
623 reached 220 mm/24h. Much better results are obtained for ALADIN 2 km model where values  
624 predicted by model were reached 200 mm/24h. A location error is also evident for both models  
625 especially for the area where most intense precipitation occurred (Istria peninsula; red dots) but it is  
626 smaller for ALADIN 2km model. Medium precipitation amounts are better forecast than strong one  
627 but still slightly overestimated for ALADIN 8 km model and much more spread is noticeable for  
628 ALADIN 2km model with both overestimation and underestimation but with better results for Istria  
629 peninsula. From Table 2 and Table 3 it can be seen that ALADIN 2 km was relatively more accurate  
630 (higher CSI) for dry and strong but not for medium category than ALADIN 8 km. FBIAS is better  
631 for ALADIN 2 km for dry and strong but also for medium category compared to ALADIN 8 km  
632 results.

633  
634  
635



636 **4.4 Influence of the data assimilation**

637

638 Since, the lack of model skill in simulating HPE may be partially attributed to imperfect initial  
639 conditions, we perform several numerical weather prediction experiments to assess the impact that  
640 data assimilation had on the IOP2 forecast accuracy.

641

642 Comparison of measurements with operational forecast and simulations without data assimilation is  
643 shown in Figure 14. Rain gauges show that along Croatia-Slovenia border elongated area of  
644 stronger precipitation is present and this pattern is better forecasted with operational run  
645 incorporating data assimilation. Also over Istria peninsula higher amounts of medium rain category  
646 are found in operational run which is in better accordance with measurements. This is also visible at  
647 Figure 13 where for run with data assimilation points are less scattered and more points with higher  
648 values of precipitation over Istria are present. Maximum recorded around the town Rijeka is not  
649 adequately represented by either of the models.

650 Verification measures (Table 2) show that slightly better results are found for simulation with data  
651 assimilation. Scores for the entire Croatia show that results in strong precipitation category are  
652 improved for operational run (CSI=0.28) compared to run without data assimilation (CSI=0.23).  
653 Also PCC shows that there is better association of model and observations for run with data  
654 assimilation. Impact of data assimilation for this IOP is rather small but it still gives improvement in  
655 24 hours precipitation forecast. It should be taken into account that for selected case better results  
656 were obtained with higher resolution model and that data assimilated in operational ALADIN 8 km  
657 model is mainly synoptic data. Thus, implementing data assimilation in higher resolution model and  
658 adding additional high resolution temporal and/or spatial data to data assimilation system seems as  
659 good way to further enhance operational forecast.

660

661

662 **Summary and conclusions**

663

664 In this paper an overview of the IOPs that affected the Adriatic TA during SOP1 HyMeX campaign  
665 (5 September to 6 November 2012) is presented. During SOP1 20 IOPs were declared and 8 of  
666 these events affected the EOP Adriatic TA. All of them produced localized heavy precipitation and  
667 often were properly forecast by the available operational model ALADIN but exact prediction of the  
668 amount, precise time and location of maximum intensity were missed. The total precipitations for  
669 the SOP1 were above the corresponding climatology for the Adriatic TA. Maximum of precipitation  
670 (more than 1.000 mm in 61 days at some locations) recorded on the northern Adriatic (city of



671 Rijeka) and its mountainous hinterland of Gorski Kotar. This region experiences climatic maxima of  
672 the annual precipitation greater than 3.000 mm on average. Analysis was done mostly by the  
673 measurements from the operational meteorological network maintained by the Meteorological and  
674 Hydrological Service of Croatia.

675 There were 15 days when the accumulated rainfall on any of the raingauges in the Adriatic TA  
676 exceeded 100 mm in 24 hours. Most the HPEs contain similar ingredients and synoptic setting but  
677 of different intensity: a deep upper level through, cyclone strengthening over the Mediterranean (or  
678 developing over Gulf of Genoa, Lyon or Tyrrhennian sea), strong southwesterly low-level jet stream  
679 that advects the moist and warm air towards the orographic obstacles along Mediterranean coastline  
680 and destabilizes the atmosphere as the strong wind picks up the moisture from the sea.

681

682 Verification of the operational precipitation forecasts during SOP 1 suggests the operational  
683 ALADIN at 8 km grid spacing model may be useful for early warnings to severe precipitation  
684 events in the region. For most of the events there was high level of association between  
685 precipitation forecast and measurements. From verification statistics and different precipitation  
686 related figures it can be seen that one obvious limitation of ALADIN 8 km model is inability to  
687 produce high amounts of precipitation and also tendency to underestimate frequency of dry events.  
688 Having model at higher resolution (ALADIN 2 km) brings improvement for both problems but now  
689 it slightly deteriorates forecast of medium precipitation and overestimates frequency of strong  
690 precipitation events. Verification methods used in this work have their limitation where for  
691 calculation of scores method used is point based comparison and thus it is prone to location error  
692 and other methods that are used based on subjective comparison of different precipitation plots.  
693 Next step would be implementation of object-based verification method e.g. SAL (Wernli et al.,  
694 2008) which could provide more objective verification measures but for this local spatial  
695 precipitation analysis must be developed first.

696

697 During the IOP2 on 12 September 2012, several thunderstorms formed including a supercell and a  
698 possible tornado outbreak. The warm and moist air advected at the low levels over the Adriatic (and  
699 Mediterranean before that) was feeding the storms, while apparently one storm produced  
700 downdrafts that would in turn form a convergence zone with the moist flow from the sea and trigger  
701 the next storm. Intensive precipitation event in Rijeka and surrounding area resulted from influence  
702 of coastal mountains on the movement of a convergence line. The atmosphere contained a lot of  
703 moisture, being close to saturated up to 6 km. The air flow converged above northern Adriatic in the  
704 layer up to 2 km. The convergence line moved south-eastward. Rainfall intensified in Rijeka area  
705 due to local terrain. The peak intensity was underestimated by the model forecast.



706

707 Such a chain of events poses a challenge with respect to predictability. The fact that the surrounding  
708 mountains represent physical obstacles that modified the flow and determined the position of the  
709 convergence zones made forecasting the location of such a chain of events easier. Abundance of real  
710 time available measured data, including radar measurements, aircraft data and targeted radio  
711 soundings can improve the initial conditions for the NWP models. The ambiguities in the sea  
712 surface fluxes that pose an important source of energy for this event could be the factor that limits  
713 the abilities of a deterministic forecast.

714

715 The numerical sensitivity experiments with respect to mesoscale data assimilation suggested the  
716 precipitation forecast during IOP 2 was improved by using data assimilation to produce initial  
717 conditions, compared to forecasts when initial conditions were derived from the global model data.  
718 Use of mesoscale data assimilation for initial conditions enhances both precipitation structure and  
719 intensity. This is evident also through improvement of objective verification measures, such as  
720 critical success index and PCC. Data assimilation system could be further enhanced by using  
721 additional observations (e.g. radar data, ground based GNSS data), shorter data assimilation cycle  
722 (e.g. 3 hours instead 6 hour) or B matrix computed with different methods (ensemble B matrix  
723 instead NMC based). Also work on implementing data assimilation system to higher resolution  
724 model is ongoing.

725 Furthermore, operational non-hydrostatic model at 2 km grid spacing is able to predict the intensity  
726 of a HPE more accurately than the hydrostatic model at 8 km grid spacing. Nevertheless, higher  
727 resolution forecast can misplace the position of the peak precipitation and overestimate precipitation  
728 over a narrow but high mountain such as southern Velebit. This may be an artefact of the excessive  
729 sea surface temperature in the model in that region. These results suggest that precipitation forecast  
730 in the Adriatic TA may be improved by both using mesoscale data assimilation and by decreasing  
731 the grid spacing of the model.

732 Heavy precipitations over Adriatic area are often associated with sirocco (*jugo*) or *bora* winds, thus  
733 involving intense air-sea interactions. In IOP4 was an excellent example for very intensive heat loss  
734 caused by strong *bora* wind. In this case, control simulation run was more realistic with colder SST  
735 and generally drier than the operational with a warmer SST. IOP4 shows the needs for further  
736 improvements of the role of SST and surface (latent and sensible) heat fluxes over the Adriatic Sea,  
737 which attain large values during strong Bora events. However a more detailed analysis of the impact  
738 of SST on precipitation is ongoing.

739

740 Therefore, this paper highlights the need for enforcement an intensive observation period in the



741 future over the Adriatic region, to better understand the relevant processes and validate the  
742 simulated mechanisms as well as to improve numerical forecasts via data assimilation and  
743 improvements of model representation of moist processes and sea-land-atmosphere interaction.  
744 There is also a need for collaborative effort within the Italian and other HyMeX scientific and  
745 forecast communities to achieve a better understanding of the complex processes caused the  
746 extreme events over the Adriatic region.

747

748

749

#### 750 **Acknowledgements**

751 *This work is a contribution to the HyMeX program. The authors are grateful to the participating*  
752 *institutions for providing the measured and model data. This work is partially supported by the Hymex-*  
753 *COOP project (ENVIMED regional programme) and IPA2007/HR/161PO/001-040510 grant. The authors*  
754 *would also like to thank Jean-Francois Geleyn (deceased) the former project manager of ALADIN*  
755 *for his ideas, energy, drive and persistence that made us an active party in developing a state of the*  
756 *art model system and enabled us to participate in such important research programme. We thank*  
757 *Marjana Gajić-Čapka for her precipitation extreme value analysis. We thank Iris Odak Plenković for*  
758 *valuable advices and suggestion regarding precipitation verification. The authors are grateful to NASA for*  
759 *providing valuable satellite derived products through the GIOVANNI web interface as well as TRMM, OMI*  
760 *and MODIS scientists and developers.*

761

762

#### 763 **References:**

764

765

766 Aladin International Team, 1997. The ALADIN project Mesoscale modelling seen as basic tool for  
767 weather forecasting and atmospheric research. *WMO Bull.* 46 : 317 - 324.

768

769 Bénard P, Vivoda J, Mašek J, Smolíková P, Yessad K, Smith Ch, Brožková R, Geleyn J-F. 2010.  
770 Dynamical kernel of the Aladin–NH spectral limited-area model: Revised formulation and  
771 sensitivity experiments. *Quart. J. R. Met. Soc.* 136 : 155 - 169. DOI: 10.1002/qj.522

772

773 Bölöni G, Horvath K, 2010. Diagnosis and tuning of background error statistics in a variational data  
774 assimilation system. *Időjárás*, 114 : 1 - 19.

775

776 Buzzi A, Tibaldi S. 1978. Cyclogenesis in the lee of the Alps: A case study. *Quart. J. R. Met. Soc.*  
777 104 : 271 - 287. DOI: 10.1002/qj.49710444004

778

779 Buzzi A, Foschini L. 2000. Mesoscale Meteorological Features Associated with Heavy Precipitation  
780 in the Southern Alpine Region. *Meteorol Atmos Phys.* 72 : 131 - 146. DOI: 10.1007/s007030050011

781

782 Catry B, Geleyn J-F, Tudor M, Benard P, Trojakova A. 2007. Flux-conservative thermodynamic  
783 equations in a mass-weighted framework. *Tellus A* 59 : 71 - 79. DOI: 10.1111/j.1600-  
784 0870.2006.00212.x

785

786 Davies, HC. 1976. A lateral boundary formulation for multi-level prediction models. *Quart. J. R.*



- 787 *Met. Soc.* 102 : 405 - 418. DOI: 10.1002/qj.49710243210  
788
- 789 Davolio S, Mastrangelo D, Miglietta MM, Drofa O, Buzzi A, Malguzzi P. 2009. High resolution  
790 simulations of a flash flood near Venice. *Nat. Hazards Earth Syst. Sci.* 9 : 1671 - 167.  
791 DOI: 10.5194/nhess-9-1671-2009  
792
- 793 Davolio S, Ferretti R, Baldini L, Casaioli M, Cimini D, Ferrario ME, Gentile S, Loglisci N, Maiello  
794 I, Manzato A, Mariani S, Marsigli C, Marzano FS, Miglietta MM, Montani A, Panegrossi G, Pasi F,  
795 Pichelli E, Pucillo A, Zinzi A. 2015. The role of the Italian scientific community in the first HyMeX  
796 SOP: an outstanding multidisciplinary experience. *Met. Zeit.* 24 : 261 - 267.  
797 DOI: 10.1127/metz/2014/0624  
798
- 799 Davolio, S, P Stocchi, A Benetazzo, E Bohm, F Riminucci, M Ravaoli, X-M Li, S Carniel, 2015.  
800 Exceptional Bora outbreak in winter 2012: Validation and analysis of high-resolution atmospheric  
801 model simulations in the northern Adriatic area. *Dynamics of Atmospheres and Oceans.* 71, 1–20.  
802
- 803 Davolio,s., Volonte A., Manzano A., Pucillo A., Cicogna A., Rerrario M.E., 2016: Mechanisms  
804 producing different precipitation patterns over north-eastern Italy: insights from HyMeX-SOP1 and  
805 previous events. *Quart. J. R. Met. Soc.*. DOI:10.1002/qj.2731  
806
- 807 Dayan, U., Nissen, K., Ulbrich, U., 2015: Review Article: Atmospheric conditions inducing extreme  
808 precipitation over the eastern and western Mediterranean. *Nat.Hazards Earth Syst. Sci.*, 15, 2525-  
809 2544.  
810
- 811 Donlon, C.J., Martin M., Stark J., Roberts-Jones, J., Fiedler, E., Wimmer, W., 2012: The operational  
812 sea surface temperature and sea ice analysis (OSTIA) system. *Remote Sens. Environ.*, 116, 140-158.  
813
- 814 Doswell, C.A., C. Ramis, R. Romero and S. Alonso (1998): A diagnostic study of three heavy  
815 precipitation episodes in the western Mediterranean. *Wea. Forecasting*, 13, 102-124.  
816  
817
- 818 Drobinski P, Ducrocq V, Alpert P, Anagnostou E, Béranger K, Borga M, Braud I, Chanzy A,  
819 Davolio S, Delrieu G, Estournel C, Filali Boubrahmi N, Font J, Grubišić V, Gualdi S, Homar V,  
820 Ivančan-Picek B, Kottmeier C, Kotroni V, Lagouvardos K, Lionello P, Llasat MC, Ludwig W,  
821 Lutoff C, Mariotti A, Richard E, Romero R, Rotunno R, Roussot O, Ruin I, Somot S, Taupier-  
822 Letage I, Tintore J, Uijlenhoet R, Wernli H. 2014. HyMeX: A 10-Year Multidisciplinary Program on  
823 the Mediterranean Water Cycle. *Bull. Amer. Meteor. Soc.*, 95 : 1063 - 1082. DOI: 10.1175/BAMS-  
824 D-12-00242.1  
825
- 826 Ducrocq V, Nuissier O, Ricard D, Lebeaupin C, Thouvenin T. 2008. A numerical study of three  
827 catastrophic precipitating events over western Mediterranean region (southern France), II:  
828 Mesoscale triggering and stationarity factors. *Quart. J. R. Met. Soc.* 134 : 131 - 145.  
829 DOI: 10.1002/qj.199  
830
- 831 Ducrocq V, Braud I, Davolio S, Ferretti R, Flamant C, Jansa A, Kalthoff N, Richard E, Taupier-  
832 Letage I, Ayrat P-A, Belamari S, Berne A, Borga M, Boudevillain B, Bock O, Boichard J-L, Bouin  
833 M-N, Bousquet O, Bouvier C, Chiggiato J, Cimini D, Corsmeier U, Coppola L, Cocquerez P, Defer  
834 E, Drobinski P, Dufournet Y, Fourrié N, Gourley JJ, Labatut L, Lambert D, Le Coz J, Marzano FS,  
835 Molinié G, Montani A, Nord G, Nuret M, Ramage K, Rison B, Roussot O, Said F, Schwarzenboeck  
836 A, Testor P, Van Baelen J, Vincendon B, Aran M, Tamayo J. 2014. HyMeX-SOP1, the field  
837 campaign dedicated to heavy precipitation and flash flooding in the northwestern Mediterranean.  
838 *Bull. Amer. Meteor. Soc.* 95 : 1083 - 1100. DOI: 10.1175/BAMS-D-12-00244.1



- 839  
840 Duffourg F, Ducrocq V. 2013. Assessment of the water supply to Mediterranean heavy precipitation:  
841 a method based on finely designed water budgets. *Atmosph. Sci. Lett.* 14 : 133 - 138.  
842 DOI: 10.1002/asl2.429  
843
- 844 Ferretti R, Pichelli E, Gentile S, Maiello I, Cimini D, Davolio S, Miglietta MM, Panegrossi G,  
845 Baldini L, Pasi F, Marzano FS, Zinzi A, Mariani S, Casaioli M, Bartolini G, Loglisci N, Montani A,  
846 Marsigli C, Manzato A, Pucillo A, Ferrario ME, Colaiuda V, Rotunno R. 2014. Overview of the first  
847 HyMeX special observation period over Italy: observations and model results. *Hydrol. Earth Syst.*  
848 *Sci.* 18 : 1953 - 1977. DOI: 10.5194/hess-18-1953-2014  
849
- 850 Geleyn J-F. 1987. Use of a modified Richardson number for parameterising the effect of shallow  
851 convection. *J. Met. Soc. Japan*. Special 1986 NWP Symposium Issue : 141-149.  
852
- 853 Geleyn J-F. 1988. Interpolation of wind, temperature and humidity values from model levels to the  
854 height of measurement. *Tellus A* 40 : 347 - 351. DOI: 10.1111/j.1600-0870.1988.tb00352.x  
855
- 856 Geleyn J-F, Bazile E, Bougeault P, Déqué M, Ivanovici V, Joly A, Labbé L, Piédelièvre J-P, Piriou  
857 J-M, Royer J-F. 1995. 'Atmospheric parametrization schemes in Météo-France's ARPEGE NWP  
858 model'. In Proceedings of the 1994 ECMWF seminar on physical parametrizations in numerical  
859 models. 385 - 402. ECMWF, Reading, UK  
860
- 861 Geleyn J-F, Hollingsworth A. 1979. An economical analytical method for the computation of the  
862 interaction between scattering and line absorption of radiation. *Contrib. Atmos. Phys.* 52 : 1 - 16.  
863
- 864 Geleyn J-F, Bénard P, Fournier R. 2005a. A general-purpose extension of the Malkmus band-model  
865 average equivalent width to the case of the Voigt line profile. *Quart. J. R. Met. Soc.* 131 : 2757 -  
866 2768. DOI: 10.1256/qj.04.107  
867
- 868 Geleyn J-F, Fournier R, Hello G, Pristov N. 2005b. 'A new 'bracketing' technique for a flexible and  
869 economical computation of thermal radiative fluxes, scattering effects included, on the basis the Net  
870 Exchanged Rate (NER) formalism.' WGNE Blue Book.  
871
- 872 Geleyn J-F, Váňa F, Cedilnik J, Tudor M, Catry B. 2006. 'An intermediate solution between  
873 diagnostic exchange coefficients and prognostic TKE methods for vertical turbulent transport.'  
874 *WGNE Blue Book*  
875
- 876 Geleyn J-F, Catry B, Bouteloup Y, Brožková R. 2008. A statistical approach for sedimentation  
877 inside a micro-physical precipitation scheme. *Tellus A* 60 : 649 - 662. DOI:  
878 10.3402/tellusa.v60i4.15375.  
879
- 880 Gerard L. 2007. An integrated package for subgrid convection, clouds and precipitation compatible  
881 with the meso-gamma scales. *Quart. J. R. Met. Soc.* 133 : 711 - 730. DOI: 10.1002/qj.58  
882
- 883 Gerard L, Geleyn J-F. 2005. Evolution of a subgrid deep convection parametrization in a limited-  
884 area model with increasing resolution. *Quart. J. R. Met. Soc.* 131 : 2293 - 2312.  
885 DOI: 10.1256/qj.04.72  
886
- 887 Gerard L, Piriou J-M, Brožková R, Geleyn J-F, Banciu D. 2009. Cloud and precipitation  
888 parameterization in a meso-gamma scale operational weather prediction model. *Mon. Wea. Rev.* 137  
889 : 3960 - 3977. DOI: 10.1175/2009MWR2750.1  
890



- 891 Giard D, Bazile E. 2000. Implementation of a new assimilation scheme for soil and surface  
892 variables in a global NWP model. *Mon. Wea. Rev.* 128 : 997 - 1015. DOI: 10.1175/1520-  
893 0493(2000)128<0997:IOANAS>2.0.CO;2
- 894
- 895 Gospodinov I, Spiridonov V, Geleyn J-F. 2001. Second order accuracy of two-time-level semi-  
896 Lagrangian schemes. *Quart. J. R. Met. Soc.* 127 : 1017 - 1033. DOI: 10.1002/qj.49712757317
- 897
- 898 Grisogono B, Belušić D. 2009. A review of recent advances in understanding the meso- and  
899 microscale properties of the severe Bora wind. *Tellus A* 61 : 1 - 16. DOI: 10.1111/j.1600-  
900 0870.2008.00369.x
- 901
- 902 Haugen JE, Machenhauer B. 1993. A spectral limited-area model formulation with time-dependent  
903 boundary conditions applied to the shallow-water equations. *Mon. Wea. Rev.* 121 : 2618 - 2630.  
904 DOI: 10.1175/1520-0493(1993)121<2618:ASLAMP>2.0.CO;2
- 905
- 906 Hollingsworth, F. Rabier and M. Fisher, 1998: The ECMWF implementation of three-dimensional  
907 variational assimilation (3d-Var). I: Formulation. *Quart. J. Roy. Meteor. Soc.*, 124, 1783-1807.
- 908
- 909 Hortal M. 2002. The development and testing of a new two-time-level semi-Lagrangian scheme  
910 (SETTLS) in the ECMWF forecast model. *Quart. J. R. Met. Soc.* 128 : 1671 - 1687.  
911 DOI: 10.1002/qj.200212858314
- 912
- 913 Horvath K, Fita LI, Romero R, Ivančan-Picek B. 2006. A numerical study of the first phase of a  
914 deep Mediterranean cyclone: Cyclogenesis in the lee of Atlas Mountains. *Met. Zeit.* 15 : 133 - 146.  
915 DOI: 10.1127/0941-2948/2006/0113
- 916
- 917 Horvath K., Lin Y-L, Ivančan-Picek B. 2008. Classification of Cyclone Tracks over Apennines and  
918 the Adriatic Sea. *Mon. Wea. Rev.* 136 : 2210 - 2227. DOI: 10.1175/2007MWR2231.1
- 919 Ivančan-Picek B, Glasnović D, Jurčec V. 2003. Analysis and ALADIN prediction of a heavy  
920 precipitation event on the Eastern side of the Alps during MAP IOP5. *Meteorol. Z.* 12 : 73 - 82.  
921 DOI: 10.1127/0941-2948/2003/0012-0103
- 922
- 923 Huffman, GJ, DT Bolvin, EJ Nelkin, DB Wolff, RF Adler, B Gu, Y Hong, KP Bowman and EF  
924 Stocker, 2007. The TRMM Multisatellite Precipitation Analysis (TMPA): quasi-global, multiyear,  
925 combined-sensor precipitation estimates at fine scales, *J. Hydrometeorol.*, 8, 38–55.
- 926
- 927 Ivančan-Picek B, Glasnović D, Jurčec V (2003) Analysis and ALADIN prediction of a heavy  
928 precipitation event on the Eastern side of the Alps during MAP IOP5. *Meteorol Z* 12:73–82.
- 929
- 930 Ivančan-Picek B, Horvath K, Strelec Mahović N, Gajić-Čapka M. 2014. Forcing mechanisms of a  
931 heavy precipitation event in the southeastern Adriatic area. *Natural hazards.* 72 : 1231 - 1252.  
932 DOI: 10.1007/s11069-014-1066-y
- 933
- 934 Jansa A, Genoves A, Picornell MA, Campins J, Riosalido R, Carretero O. 2001. Western  
935 Mediterranean cyclones and heavy rain. Part 2: Statistical approach. *Met. Apps.* 8 : 43 - 56.  
936 DOI: 10.1017/S1350482701001049
- 937
- 938 Jeromel M, Malačić V, Rakovec J. 2009. Weibull distribution of bora and sirocco winds in the  
939 northern Adriatic Sea, *Geofizika*, 26 : 85 - 100.
- 940
- 941 Juras, J., Pasarić, Z., 2006. *Application of tetrachoric and polychoric correlation*  
942 *coefficients to forecast verification.* *Geofizika*, 23, 59–81.



- 943  
944 Jurčec V, Ivančan-Picek B, Tutiš V, Vukičević V. 1996. Severe Adriatic jugo wind. *Met. Zeit.* 5 : 67  
945 - 75.  
946  
947 Kozarić T, Ivančan-Picek B. 2006. Meteorological features of extreme precipitation in the Northern  
948 Adriatic. *Croat. Met. J.* 41: 53 - 67.  
949  
950 Louis J-F, Tiedke M, Geleyn J-F. 1982. `A short history of PBL parameterization at ECMWF.` In  
951 Proceedings from ECMWF workshop on planetary boundary layer parameterization, 25–27  
952 November 1981, pp 59–79, ECMWF, Reading, UK.  
953  
954 Lorenc, A. C., 1986. Analysis methods for numerical weather prediction. *Quart. J. R. Met. Soc.*,  
955 112, 1177-1194. DOI: 10.1002/qj.49711247414  
956  
957 Machenhauer B, Haugen JE. 1987. `Test of a spectral limited area shallow water model with time-  
958 dependent lateral boundary conditions and combined normal mode/semi-Lagrangian time  
959 integration schemes.` Workshop on Techniques for Horizontal Discretization in Numerical Weather  
960 Prediction Models, 2-4 November 1987, ECMWF, Reading, UK  
961  
962 Magaš D. 2002: Natural-geographic characteristics of the Boka Kotorska area as the basis of  
963 development, *Geoadria*, 7 : 51 - 81.  
964  
965 Maiello I, Ferretti R, Baldini L, Roberto N, Picciotti E, Gentile S, Alberoni PP, Marzano FS. 2014.  
966 `Multiple Doppler radar data assimilation with WRF 3d-VAR: IOP4 of HyMeX campaign  
967 retrospective studies.` In Proceedings of 8th European Conference on Radar in Meteorology and  
968 Hydrology, 1 - 5 September 2014, Garmisch-Partenkirchen, Germany. ERAD 2014 Abstract ID  
969 042.  
970  
971 Manzato A, Davolio S, Miglietta MM, Pucillo A, Setvak M. 2015. 12 September 2012: A supercell  
972 outbreak in NE Italy? *Atmos. Res.* 153 : 98 - 118. DOI: 10.1016/j.atmosres.2014.07.019  
973  
974 Mastrangelo D, Horvath K, Riccio A, Miglietta MM. 2011. Mechanisms for convection  
975 development in a long-lasting heavy precipitation event over southeastern Italy. *Atmos. Res.* 100 :  
976 586 - 602. DOI: 10.1016/j.atmosres.2010.10.010  
977  
978 Mikuš P, Telišman Prtenjak M, Strelec Mahović N. 2012. Analysis of the convective activity and its  
979 synoptic background over Croatia. *Atmos Res.* 104-105: 139 - 153.  
980 DOI: 10.1016/j.atmosres.2011.09.016  
981  
982 Noilhan J, Planton S. 1989. A Simple Parameterization of Land Surface Processes for  
983 Meteorological Models. *Mon. Wea. Rev.* 117 : 536 - 549. DOI: 10.1175/1520-  
984 0493(1989)117<0536:ASPOLS>2.0.CO;2  
985  
986 Orlić M, Kuzmić M, Pasarić Z. 1994. Response of the Adriatic Sea to the bora and sirocco forcing.  
987 *Cont. Shelf. Res.*, 14 : 91 - 116. DOI: 10.1016/0278-4343(94)90007-8  
988  
989 Pandžić K, and Likso T. 2005. Eastern Adriatic typical wind field patterns and large-scale  
990 atmospheric conditions. *Int. J. Climatol.* 25 : 81 - 98. DOI: 10.1002/joc.1085  
991  
992 Pantillon F, Chaboureaud J-P, Richard E. 2015. Remote impact of North Atlantic hurricanes on the  
993 Mediterranean during episodes of intense rainfall in autumn 2012. *Quart. J. R. Met. Soc.* 141 : 967 -  
994 978. DOI: 10.1002/qj.2419



- 995  
996 Parrish DF, Derber JC. 1992. The National Meteorological Center's Spectral Statistical-Interpolation  
997 Analysis System. *Mon. Wea. Rev.* 120 : 1747 - 1763. DOI: 10.1175/1520-  
998 0493(1992)120<1747:TNMCSS>2.0.CO;2  
999  
1000 Patarčić M, Gajić-Čapka M, Cindrić K, Branković Č. 2014. Recent and near-future changes in  
1001 precipitation-extreme indices over the Croatian Adriatic coast. *Clim. Res.* 61 : 157 - 176.  
1002 DOI: 10.3354/cr01250  
1003  
1004 Prates, C., D. Richardson, C.Sahin, 2009: Final report of the PREVIEW observation Data targeting  
1005 System (DTS). *ECMWF, Technical Memorandum*, no. 581.  
1006  
1007 Radnóti, G., 1995. Comments on "A spectral limited-area formulation with time-dependent  
1008 boundary conditions applied to the shallow-water equations". *Mon. Wea. Rev.*, 123, 3122– 3123.  
1009  
1010 Reborá N, Molini L, Casella E, Comellas A, Fiori E, Pignone F, Siccardi F, Silvestro F, Tanelli S,  
1011 Parodi A. 2013: Extreme Rainfall in the Mediterranean: What Can We Learn from Observations?. *J.*  
1012 *Hydrometeor.* 14 : 906 - 922. DOI: 10.1175/JHM-D-12-083.1  
1013  
1014 Renko T, Kozarić T, Tudor M. 2012. An assessment of waterspout occurrence in the Eastern  
1015 Adriatic basin in 2010 : Synoptic and mesoscale environment and forecasting method. *Atmos Res.*  
1016 123 : 71 - 81. DOI: 10.1016/j.atmosres.2012.06.018  
1017  
1018 Ricchi A., Miglietta M.M., Falco P.P., Benetazzo A., Bonaldo D., Bergamasco A., Sclavo M.,  
1019 Carniel S., 2016: On the use of a coupled ocean-atmosphere-wave model during an extreme cold air  
1020 outbreak over the Adriatic Sea. *Atmospheric Research*. DOI: 10.1016/j.atmosres.2015.12.023  
1021  
1022 Ritter B, Geleyn J-F. 1992. A Comprehensive Radiation Scheme for Numerical Weather Prediction  
1023 Models with Potential Applications in Climate Simulations. *Mon. Weather Rev.* 120 : 303 - 325  
1024 DOI: 10.1175/1520-0493(1992)120<0303:ACRSFN>2.0.CO;2  
1025  
1026 Robert A. 1982. A semi-Lagrangian and semi-implicit numerical integration scheme for the  
1027 primitive equations. *J. Meteor. Soc. Japan.* 60 : 319 - 325.  
1028  
1029 Romero R, Doswell III CA, Ramis C, 2000. Mesoscale numerical study of two cases of long-lived  
1030 quasi-stationary convective systems over eastern Spain. *Mon. Wea. Rev.* 128 : 3731 - 3752.  
1031 DOI: 10.1175/1520-0493(2001)129<3731:MNSOTC>2.0.CO;2  
1032  
1033 Romero, R., C. Ramis, S. Alonso, C.A. Doswell III and D. J. Stensrud (1998): Mesoscale model  
1034 simulations of three heavy precipitation events in the western Mediterranean region. *Mon. Wea.*  
1035 *Rev.*, 126, 1859-1881.  
1036  
1037 Rotunno R, Ferretti R. 2001. Mechanisms of Intense Alpine Rainfall. *J. Atmos. Sci.* 58 : 1732 -  
1038 1749. DOI: 10.1175/1520-0469(2001)058<1732:MOIAR>2.0.CO;2  
1039  
1040 Silvestro F, Gabellani S, Giannoni F, Parodi A, Reborá N, Rudari R, Siccardi F. 2012. A  
1041 hydrological analysis of the 4 November 2011 event in Genoa. *Nat. Hazards Earth Syst. Sci.* 12 :  
1042 2743 - 2752. DOI: 10.5194/nhess-12-2743-2012  
1043  
1044 Simmons AJ, Burridge DM. 1981. An Energy and Angular-Momentum Conserving Vertical Finite-  
1045 Difference Scheme and Hybrid Vertical Coordinates. *Mon. Wea. Rev.* 109 : 758 - 766.  
1046 DOI: [http://dx.doi.org/10.1175/1520-0493\(1981\)109<0758:AEAAMC>2.0.CO;2](http://dx.doi.org/10.1175/1520-0493(1981)109<0758:AEAAMC>2.0.CO;2)



- 1047  
1048 Stanešić, A. 2011. Assimilation system at DHMZ: Development and first verification results. *Croat.*  
1049 *Met. J.* 44/45 : 3 - 17.  
1050  
1051 Stocchi P., S. Davolio, 2016: Intense air-sea exchange and heavy rainfall: impact of the northern  
1052 Adriatic SST. *Adv. Sci. Res.*, 13, 7-12. DOI: 10.5194/asr-13-7-2016  
1053  
1054 Termonia P, 2008: Scale-Selective Digital-Filtering Initialization. *Mon. Wea. Rev.* 136 : 5246 - 5255.  
1055 DOI: 10.1175/2008MWR2606.1  
1056  
1057 Tudor M, Ivatek-Šahdan S. 2010. The case study of bura of 1<sup>st</sup> and 3<sup>rd</sup> February 2007, *Met. Zeit.* 19  
1058 : 453 - 466. DOI: 10.1127/0941-2948/2010/0475  
1059  
1060 Tudor M, Ivatek-Šahdan S, Stanešić A, Horvath K, Bajić A. 2013. *Forecasting weather in Croatia*  
1061 *using ALADIN numerical weather prediction model. In: Climate Change and Regional/Local*  
1062 *Responses / Zhang, Yuanzhi ; Ray, Pallav (eds.). InTech: Rijeka; pp 59-88.*  
1063  
1064 Váňa F, Bénard P, Geleyn J-F, Simon A, Seity Y. 2008. Semi-Lagrangian advection scheme with  
1065 controlled damping—an alternative way to nonlinear horizontal diffusion in a numerical weather  
1066 prediction model. *Quart. J. R. Met. Soc.* 134 : 523 - 537. DOI: 10.1002/qj.220  
1067  
1068 Vrhovec T, Gregorič G, Rakovec J, Žagar M. 2001. Observed versus forecasted precipitation in the  
1069 South East Alps. *Met. Zeit.* 10 :17 - 27. DOI: 10.1127/0941-2948/2001/0010-0017  
1070  
1071 Wernli H, Paulat M, Hagen M, Frei C. 2008. SAL—A novel quality measure for the verification of  
1072 quantitative precipitation forecasts. *Mon. Weather Rev.* 136: 4470–4487.  
1073  
1074 Wilks DS. 2006. *Statistical Methods in the Atmospheric Sciences.* Academic Press: London; 676 pp.  
1075  
1076 Zaninović K, Gajić-Čapka M, Perčec Tadić M, Vučetić M, Milković J, Bajić A, Cindrić K, Cvitan  
1077 L, Katusin Z, Kaučić D, Likso T, Lončar E, Lončar Ž, Mihajlović D, Pandžić K, Patarčić, M, Srnc  
1078 L, Vučetić V. 2008. *Climate atlas of Croatia 1961-1990., 1971-2000.* Meteorological and  
1079 Hydrological Service: Zagreb  
1080  
1081  
1082  
1083  
1084  
1085  
1086  
1087  
1088  
1089  
1090  
1091  
1092  
1093  
1094  
1095  
1096  
1097  
1098  
1099  
1100



1101 **List of Tables:**

1102  
 1103

1104 **Table 1:** *HPEs over the Adriatic TA during SOP1. The column titled Rainfall lists the maximum 24*  
 1105 *hour accumulated precipitation (from 0600 UTC to 0600 UTC). Weather regime gives associated*  
 1106 *large scale weather.*

1107

Date	IOP	Location	Rainfall (mm)	Weather regime
12-13 Sep	2	Rijeka	220.2	NAO+, cold front, SW advection
13-14 Sep	4	Pelješac	101.4	NAO+, cyclone, bora and sirocco
1-2 Oct	9	Rijeka	127.4	NAO+, cold front, SW advection
11-13 Oct	12a	Silba, Šolta, Prevlaka	121.0	blocking, cold front, SW advection
14-16 Oct	13	Hvar, Mljet, Rijeka, Karlobag, Imotski	118.6, 145.4	blocking, cold front, SW advection
26-28 Oct	16	Rijeka, Rijeka inland	180.1, 173.5	NAO-, blocking, cyclone, sirocco, aqua alta
31Oct-2 Nov	18	Istria, Rijeka	171.4	NAO-, cyclone, sirocco, aqua alta
4-5 Nov	19	Rijeka inland	177.0	NAO-, cyclone, SW advection

1108

1109

1110

1111

1112

1113

1114

1115

1116

1117

1118

1119

1120

1121

1122

1123

1124

1125

1126

1127

1128

1129

1130



1131 **Table 2:** Verification measures calculated for 24 hour accumulated precipitation and for ALADIN 8 km  
 1132 model (second column) for three categories (first column) and for whole SOP1 period (5 September to 6  
 1133 November 2012), only IOP days (IOPavg) and for selected (IOP)s corresponding to time periods indicated  
 1134 in Table 1 and for IOP2 without data assimilation experiment (IOP2 no DA). Verification measures include  
 1135 Base Rate (BR), Frequency Bias (FBIAS), Critical Success Index (CSI) and polychoric correlation coefficient  
 1136 (PCC). Due to zeros in contingency table some PCC scores could not be calculated (IOP4 and IOP16 for  
 1137 ALADIN 8km model).

Cat.	Measure	Period										
		SOP1	IOPavg	IOP2	IOP2 no DA	IOP4	IOP9	IOP12a	IOP13	IOP16	IOP18	IOP19
Dry	BR [%]	64.7	18.1	15.5	15.5	2.7	12.7	27	30.9	2.9	10.6	44.7
	FBIAS	0.78	0.29	0.5	0.41	0	0.15	0.47	0.45	0	0.01	0
	CSI	0.73	0.23	0.16	0.16	0	0.08	0.39	0.41	0	0.01	0
Medium	BR [%]	33.6	74.5	60.1	60.1	86.9	86.4	69.8	62.9	87.9	85.1	49.6
	FBIAS	1.45	1.2	1.36	1.39	1.03	1.1	1.24	1.26	1.09	1.14	1.91
	CSI	0.62	0.76	0.59	0.59	0.84	0.84	0.76	0.65	0.88	0.86	0.5
Strong	BR [%]	1.8	7.3	24.3	24.3	10.4	0.8	3.3	6.3	9.3	4.3	5.7
	FBIAS	0.63	0.73	0.42	0.42	0.98	3.75	0.19	1.13	0.42	0.69	0.89
	CSI	0.2	0.23	0.28	0.23	0.22	0	0	0.08	0.19	0.39	0.39
	PCC	0.8987	0.6847	0.5926	0.5488	-	0.3265	0.7489	0.7056	-	0.8824	0.7182

1138  
 1139  
 1140  
 1141

**Table 3:** Same as Table 2 but verification measures are calculated for ALADIN 2 km model.

Cat.	Measure	Period									
		SOP1	IOPavg	IOP2	IOP4	IOP9	IOP12a	IOP13	IOP16	IOP18	IOP19
Dry	BR [%]	64.7	18.1	15.5	2.7	12.7	27.0	30.9	2.9	10.6	44.7
	FBIAS	0.92	0.81	0.83	1.69	1.29	0.76	0.74	0.79	0.64	0.84
	CSI	0.78	0.39	0.18	0.00	0.15	0.39	0.59	0.19	0.04	0.68
Medium	BR [%]	33.6	74.5	60.1	86.9	86.4	69.8	62.9	87.9	85.1	49.6
	FBIAS	1.12	1.00	1.11	0.85	0.86	1.12	1.07	0.98	1.01	1.09
	CSI	0.59	0.71	0.50	0.70	0.69	0.73	0.69	0.83	0.76	0.64
Strong	BR [%]	1.8	7.3	24.3	10.4	0.8	3.3	6.3	9.3	4.3	5.7
	FBIAS	1.65	1.49	0.84	2.08	10.75	0.38	1.64	1.22	1.76	1.46
	CSI	0.17	0.20	0.32	0.21	0.00	0.05	0.21	0.18	0.18	0.19
	PCC	0.8407	0.624	0.5302	0.3987	0.2083	0.4933	0.7896	0.3233	0.326	0.7854

1142



1143

1144 **Table 4:** Annual maximal precipitation amounts ( $R_{max}$ ) recorded in different intervals  $t$  (minutes)  
 1145 throughout the period 1958-2011 and during the heavy rainfall event on September 12, 2012 at  
 1146 Rijeka and their return values ( $T$ ) according to the GEV distribution applied to the period 1958-  
 1147 2011.  
 1148

t (minutes)	1958-2011		12 Sept 2012	$T_{1958-2011}$
	$R_{max}$ (mm)	T (year)		
5 min	19.3	50	14.5	7
10 min	29.2	54	24.6	12
20 min	40.2	63	<b>46.7</b>	>1000
30 min	55.5	69	<b>63.7</b>	415
40 min	67	48	<b>74.8</b>	130
50 min	77.8	40	<b>80.8</b>	62
60 min	86.4	40	<b>87.4</b>	43
120 min	138.9	38	<b>141.1</b>	40
4 h	194.9	80	171.8	52
6 h	252.5	103	181.5	36
12 h	317.3	214	200.9	37
18 h	324.7	228	205.3	29
24 h	324.7	232	208.3	25

1149  
 1150  
 1151  
 1152  
 1153  
 1154  
 1155  
 1156  
 1157  
 1158  
 1159  
 1160  
 1161  
 1162  
 1163  
 1164  
 1165  
 1166  
 1167  
 1168  
 1169  
 1170  
 1171  
 1172  
 1173  
 1174  
 1175  
 1176  
 1177  
 1178  
 1179  
 1180  
 1181



1182 **List of figures:**

1183

1184 **Figure 1:** ALADIN model domain and terrain height in 8 km (a) and 2 km (b) horizontal resolution.

1185

1186 **Figure 2:** a) Total precipitation measured by the Croatian rain gauge network, cumulated over the  
1187 whole SOP1 period; b) Maximum 24-h rainfall totals at each rain gauge station during the SOP1.

1188

1189 **Figure 3:** Horizontal wind at 10 m (arrows coloured according to wind speed) and mean sea level  
1190 pressure (blue isolines) forecasts by the ALADIN 8 km resolution run for 1200 UTC for: a) IOP4  
1191 (13 September); b) IOP9 (1 October); c) IOP13 (15 October); d) IOP16 (27 October); e) IOP18  
1192 (31 October); f) IOP19 (4 November).

1193

1194 **Figure 4:**

1195 A - IOP13 (16 October): accumulated 24 hourly rainfall measured on rain gauges (circles) and  
1196 interpolated using data from rain gauges and 3B42RT3 hourly product for periods starting at 0600  
1197 UTC (a); accumulated 24 hourly precipitation forecasts from the ALADIN 8 km resolution run  
1198 (starting from 000 UTC on the same day) and for ALADIN 2 km resolution run (c).

1199 B: same as A but for IOP16 (28 October)

1200 C: same as A but for IOP18 (1 November)

1201 D: same as A but for IOP19 (4 November)

1202

1203 **Figure 5:** Radiosounding data for Zadar 26 October 2012 at 0600 and 1200 UTC (first row), 26  
1204 October 2012 at 1800 and 27 October 2012 at 0000 UTC (second row).

1205

1206 **Figure 6:** a) Sea surface temperature measured in situ (red) on station Bakar close to the city of  
1207 Rijeka and the nearest sea point data used in the ALADIN 8 km resolution model from the global  
1208 ARPEGE model (light blue) and OSTIA (blue) for the SOP1 from 5 September to 8 November 2012.  
1209 For IOP4 (14 September) b) Accumulated 24 hourly rainfall measured on rain gauges (circles) and  
1210 interpolated using data from rain gauges and 3B42RT3 hourly product for periods starting at 0600  
1211 UTC; c) accumulated 24 hourly precipitation forecasts from the ALADIN 8 km resolution; d)  
1212 accumulated 24 hourly precipitation forecasts from the ALADIN 2 km resolution run with SST from  
1213 OSTIA; e) accumulated 24 hourly precipitation forecasts from the ALADIN 2 km resolution with  
1214 SST from ARPEGE global model.

1215

1216 **Figure 7:** Normalized histogram of rain events (24h accumulated precipitation on rain gauge  
1217 station greater or equal 0.2 mm/24h) for the whole SOP1 period (5 September to 6 November 2012)  
1218 (left column) and for days of selected (IOP)s within the same period (right column). In order to  
1219 have readable histogram first histogram bin starts from 0.2 mm while number of dry days for given  
1220 period is indicated at graph. Location of 95<sup>th</sup> percentile of SOP1 rain events distribution (50.42  
1221 mm/24h) is shown. Area of histogram after 95<sup>th</sup> percentile is zoomed and shown as inset to enhance  
1222 readability. Frequency of precipitation events for rain gauge is coloured blue, for model light green,  
1223 while dark green indicates overlapping of model and rain gauge data. First row: ALADIN 8km,  
1224 Second row: ALADIN 2km upscaled to ALADIN 8km grid.

1225

1226 **Figure 8:** Mean sea level pressure (a) and 850 hPa geopotential height (blue isolines), wind speed  
1227 (background shading) and direction (vectors) (b) according to the ALADIN model operational  
1228 forecast on 2100 UTC 12 September 2012 (starting from the 0000 UTC analysis of the same day).

1229

1230 **Figure 9:** Hour precipitation amounts from 1pm on 12 September 2012 to 1 pm on September 13,  
1231 2012 recorded at the Rijeka meteorological station.

1232



1233 **Figure 10:** IR temperature enhanced satellite image for 2100 UTC on 12 Sep 2012 operational  
1234 MSG product used in DHMZ at the time.

1235

1236 **Figure 11:** High resolution forecast of hourly accumulated precipitation (shaded background) and  
1237 TRMM 3B41RT precipitation estimates (squares) for 1900 (a), 2000 (b), 2100 (c), 2200 (d) and  
1238 2300 (e) UTC 12 and 0000 (f) UTC 13 September 2012, this was the period of highest precipitation  
1239 intensity. Satellite derived precipitation data are used as provided from the Tropical Rainfall Measuring  
1240 Mission (TRMM, (Huffman et al. 2007)), in particular we used the hourly precipitation intensity data from  
1241 3B41RT product.

1242

1243 **Figure 12:** Vertical velocity omega (Pa/s) at 850 hPa level from the operational 2 km resolution  
1244 forecast for 2200 (a) and 2300 (b) UTC on 12 and 0000 (c) and 0100 (d) UTC on 13 September  
1245 2012, upward motions are shown in shades of red and downward in blue.

1246

1247

1248 **Figure 13:** Scatter plot of 24h accumulated precipitation from rain gauges over Croatia and model  
1249 equivalent from ALADIN 8 km (left), ALADIN 8 km without data assimilation (middle), ALADIN 2  
1250 km (right) model and from the point nearest to the location of rain gauge for IOP2. With red colour  
1251 locations from Istria peninsula are marked.

1252

**Figure 14:** 24h accumulated precipitation from 12 Sep 0600 UTC until 13 Sep 0600 UTC (IOP12).  
Left: rain gauge measurement, middle: ALADIN 8 km operational forecast with data assimilation,  
right: ALADIN 8 km forecast without data assimilation.

1253

1254

1255

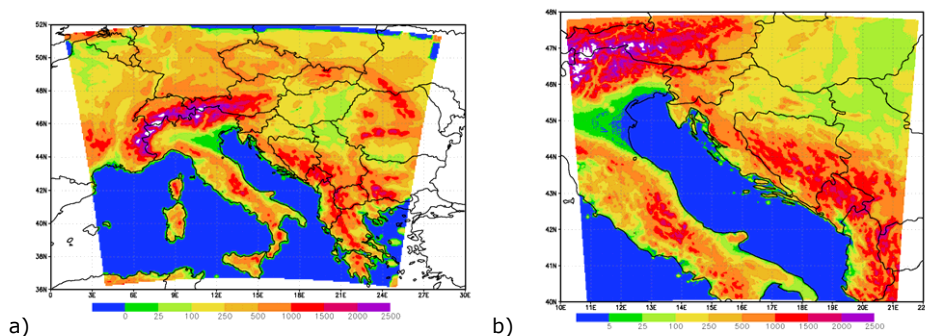
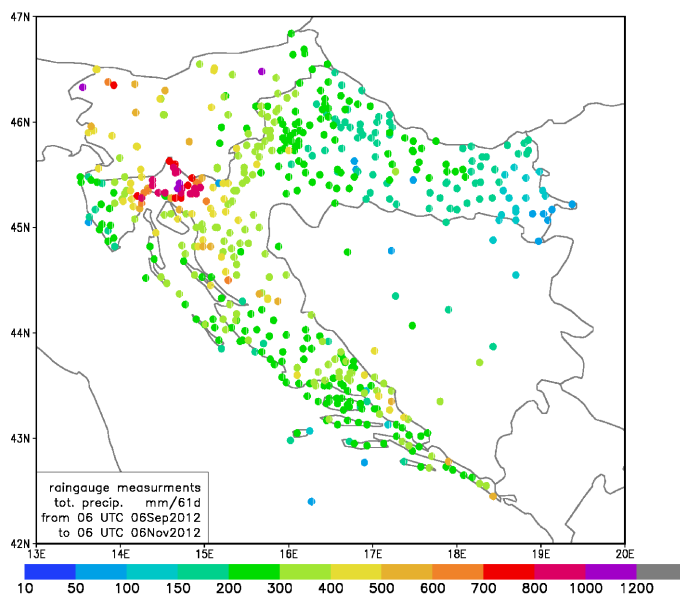
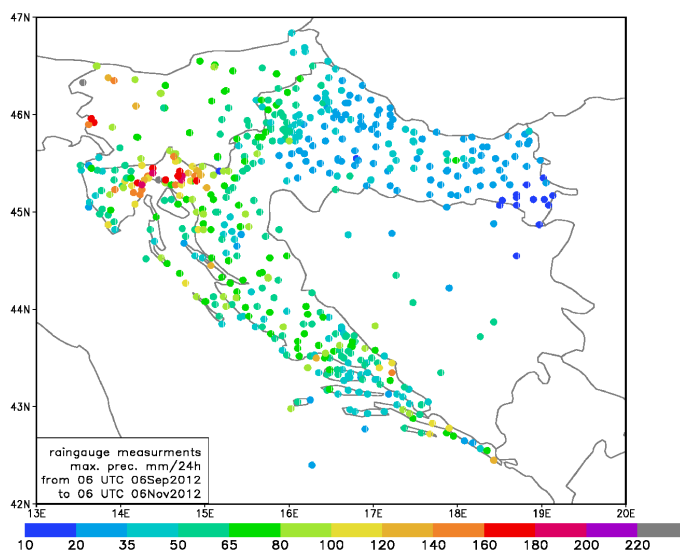


**Figure 1:** ALADIN model domain and terrain height in 8 km (a) and 2 km (b) horizontal resolution.



a)



b)

**Figure 2:** a) Total precipitation measured by the Croatian rain gauge network, cumulated over the whole SOP1 period; b) Maximum 24-h rainfall totals at each rain gauge station during the SOP1.



**Figure 3**

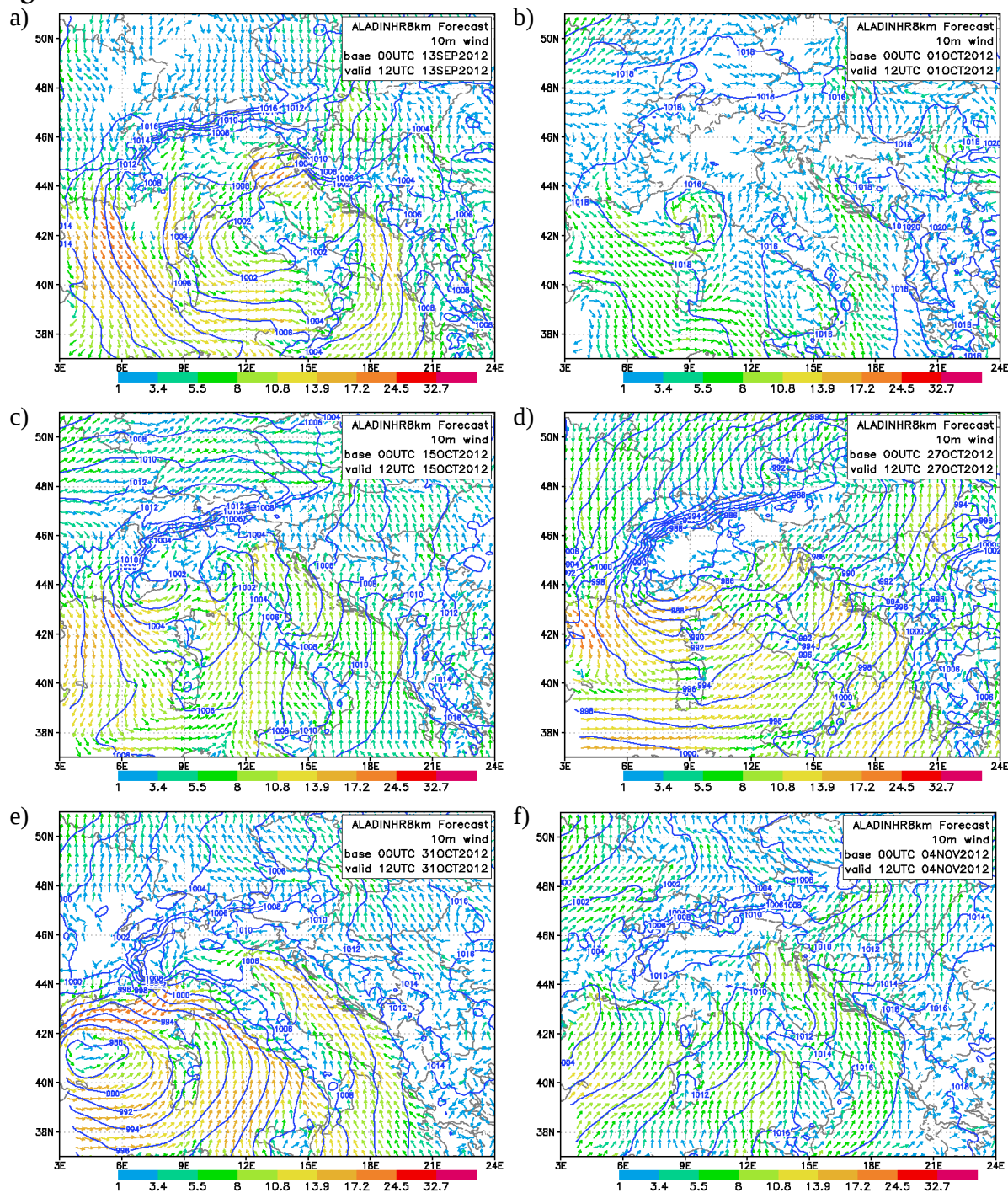


Figure 3: Horizontal wind at 10 m (arrows coloured according to wind speed) and mean sea level pressure (blue isolines) forecasts by the ALADIN 8 km resolution run for 1200 UTC for: a) IOP4 (13 September); b) IOP9 (1 October); c) IOP13 (15 October); d) IOP16 (27 October); e) IOP18 (31 October); f) IOP19 (4 November). □



**Figure 4A**

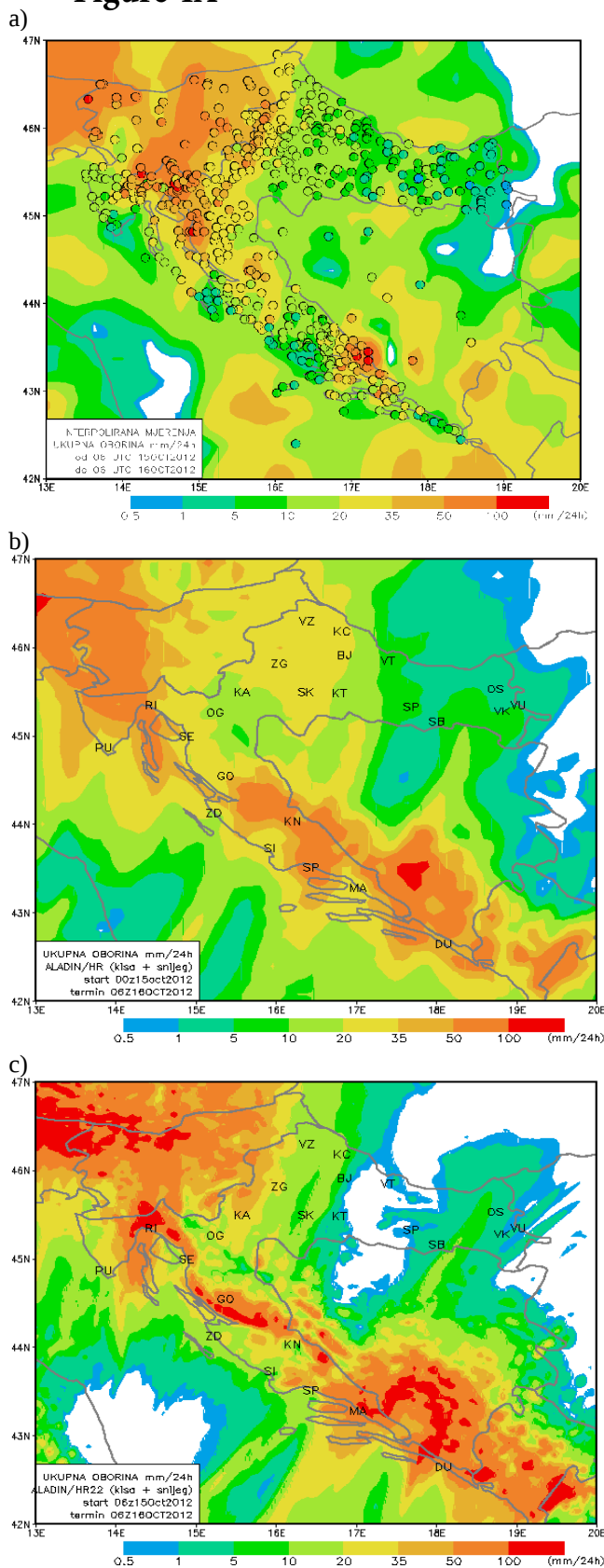
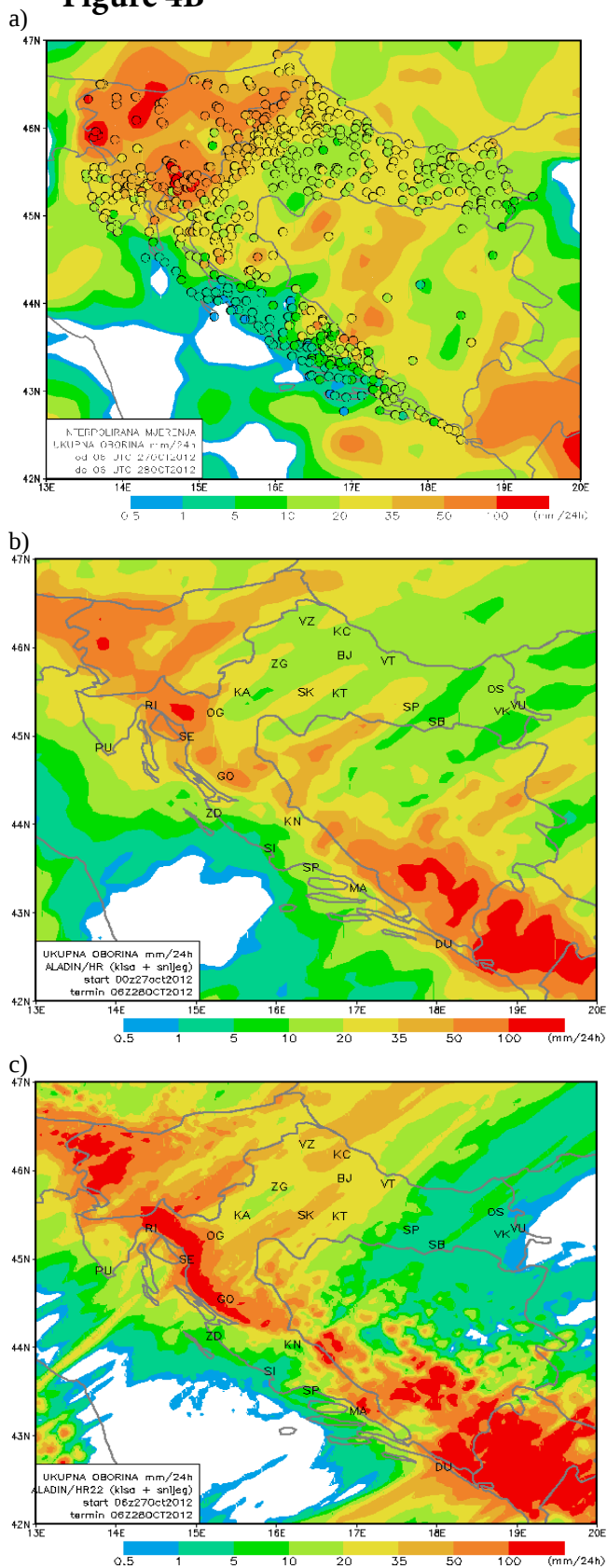


Figure 4: A - IOP13 (16 October): accumulated 24 hourly rainfall measured on rain gauges (circles) and interpolated using data from rain gauges and a cumulated 3B42RT 3 hourly product for periods starting at 0600 UTC (a); accumulated 24 hourly precipitation forecasts from the ALADIN 8 km resolution run (starting from 00 UTC on the same day) (b) and for ALADIN 2 km resolution run (c).



**Figure 4B**



*Figure 4*  
*B: same as A but for IOP16 (28 October) □*



**Figure 4C**

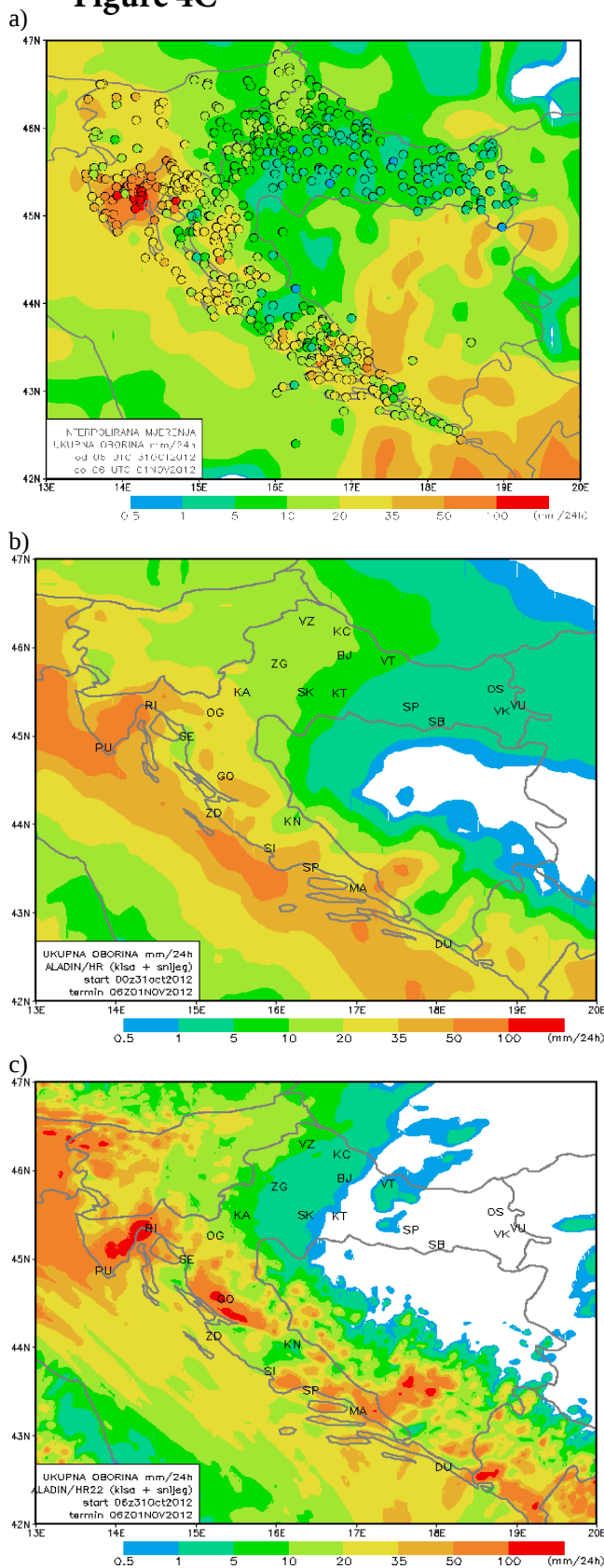


Figure 4  
 C: same as A but for IOP18 (1 November) □



a) **Figure 4D**

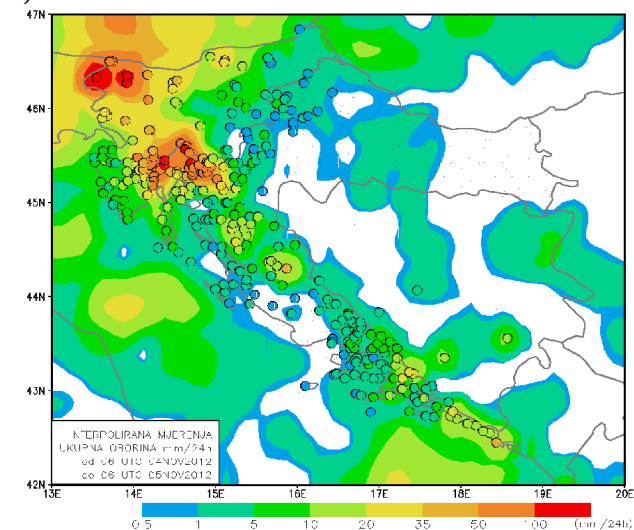


Figure 4  
 D: same as A but for IOP 19 (4 November)

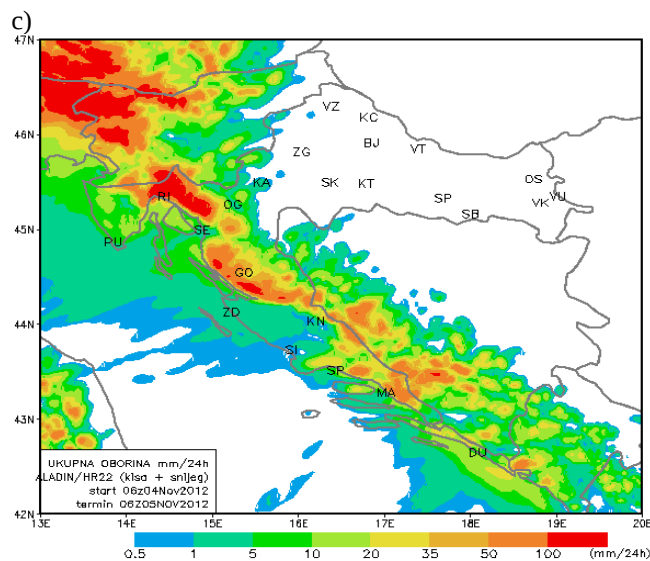
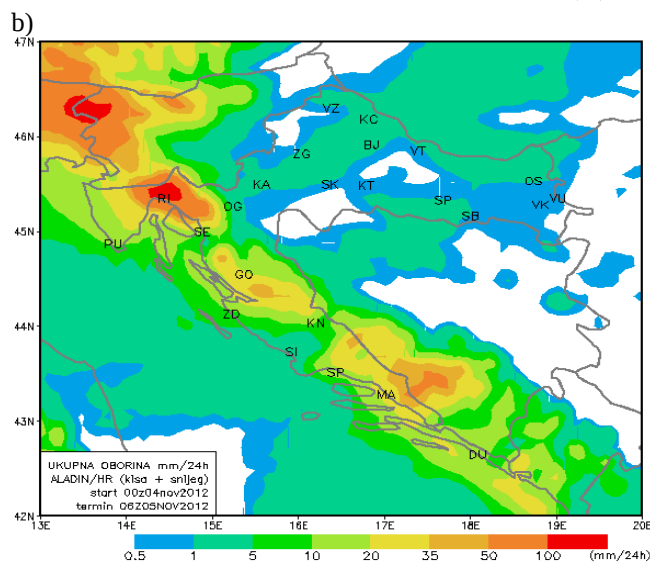




Figure 5

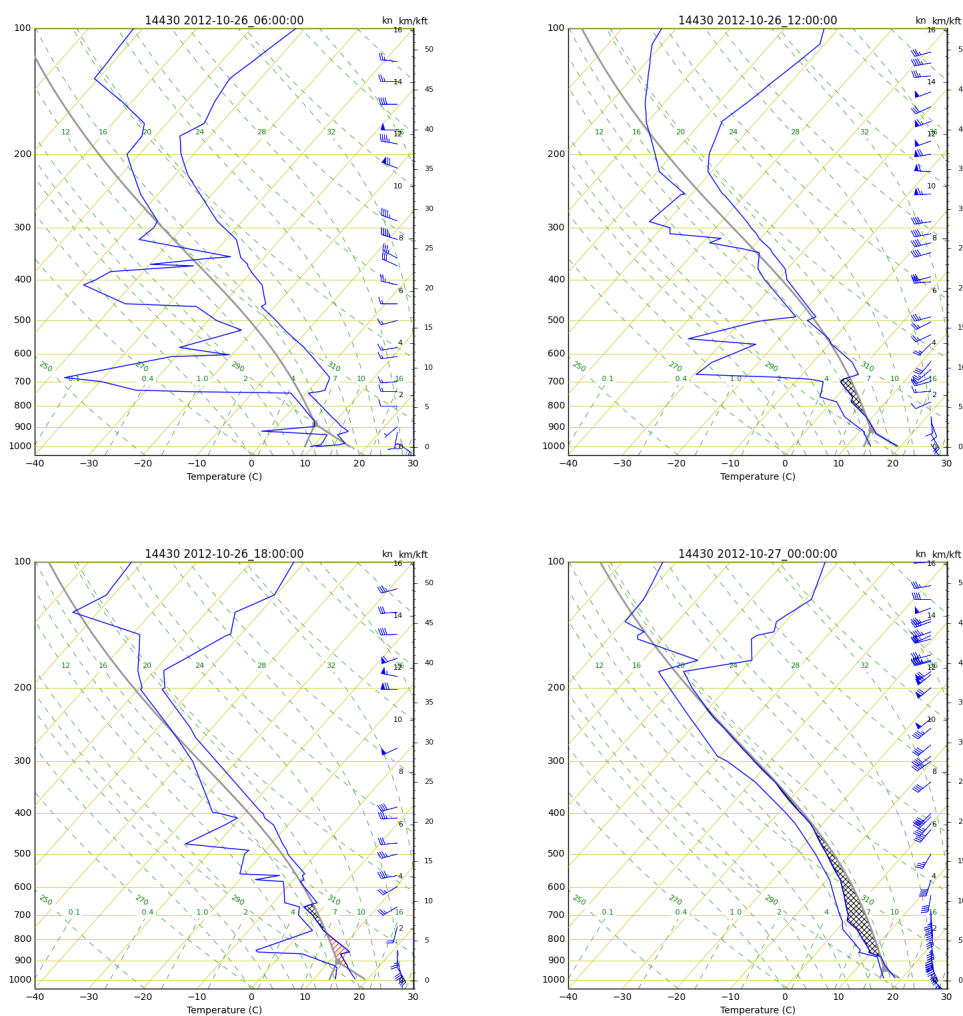


Figure 5: Radiosounding data for Zadar 26 October 2012 at 0600 and 1200 UTC (first row), 26 October 2012 at 1800 and 27 October 2012 at 0000 UTC (second row).



**Figure 6**

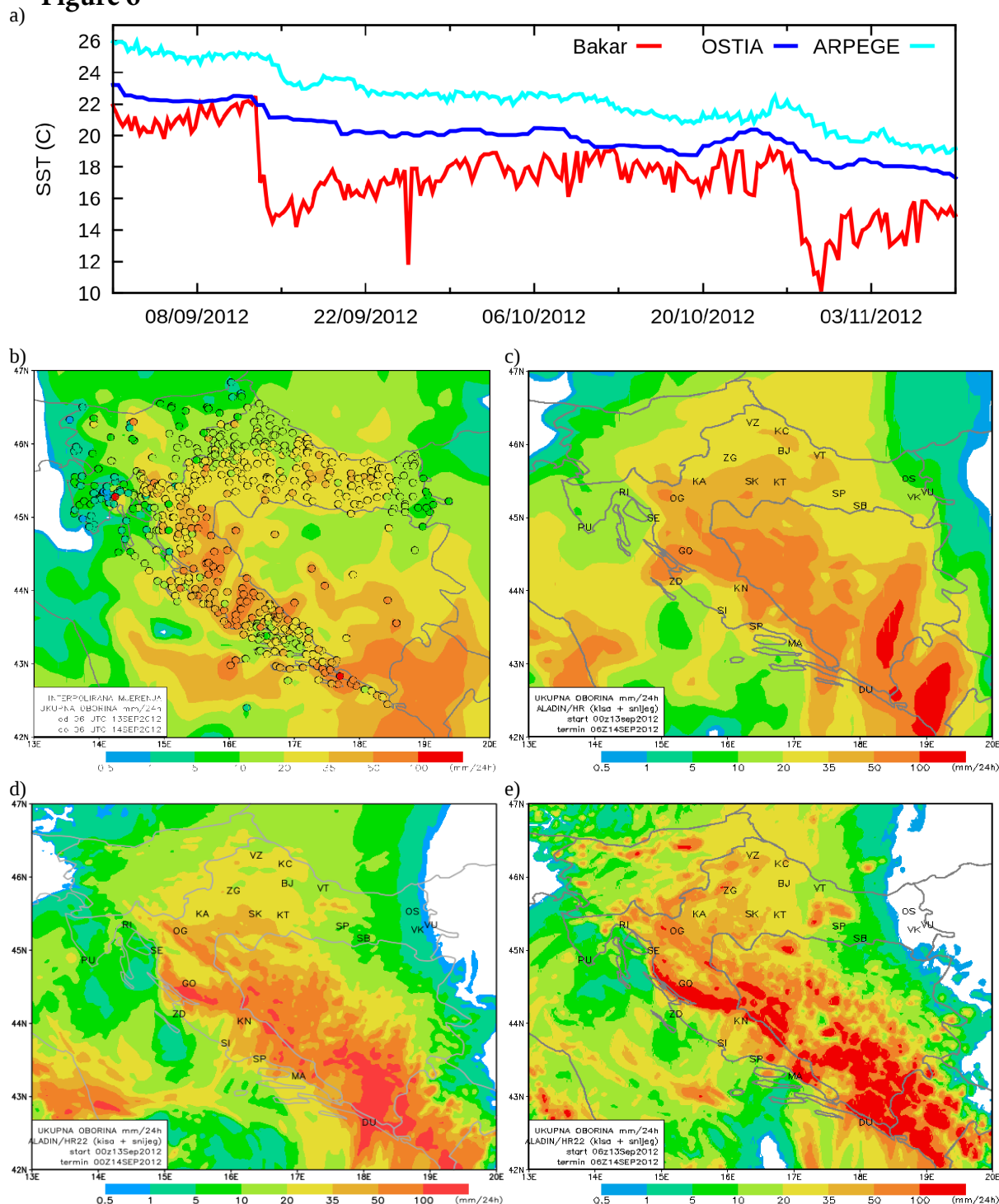
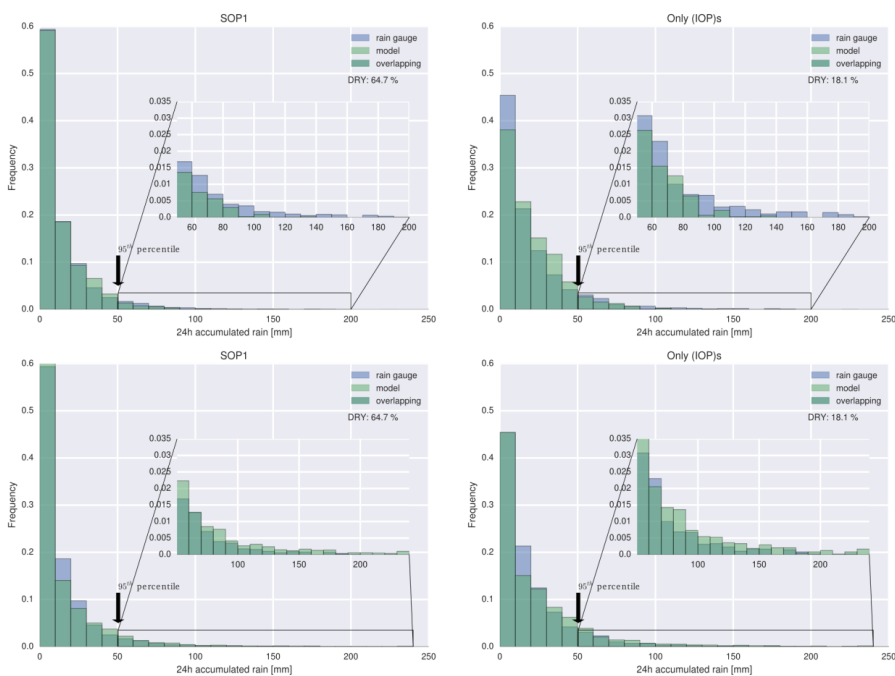


Figure 6: a) Sea surface temperature measured in situ (red) on station Bakar close to the city of Rijeka and the nearest sea point data used in the ALADIN 8 km resolution model from the global ARPEGE model (light blue) and OSTIA (blue) for the SOP1 from 5 September to 8 November 2012. For IOP4 (14 September) b) Accumulated 24 hourly rainfall measured on rain gauges (circles) and interpolated using data from rain gauges and 3B42RT 3 hourly forecasts for periods starting at 0600 UTC; c) accumulated 24 hourly precipitation forecasts from the ALADIN 8 km resolution; d) accumulated 24 hourly precipitation forecasts from the ALADIN 2 km resolution run with SST from OSTIA; e) accumulated 24 hourly precipitation forecasts from the ALADIN 2 km resolution with SST from ARPEGE global model. □



**Figure 7:** Normalized histogram of rain events (accumulated precipitation on rain gauge station greater or equal 0.2 mm/24h) for the whole SOP1 period (5 September to 6 November 2012) (left column) and for days of selected (IOP)s within the same period (right column). In order to have readable histogram first histogram bin starts from 0.2 mm while number of dry days for given period is indicated at graph. Location of 95<sup>th</sup> percentile of SOP1 rain events distribution (50.42 mm/24h) is shown. Area of histogram after 95<sup>th</sup> percentile is zoomed and shown as inset to enhance readability. Frequency of precipitation events for rain gauge is coloured blue, for model light green, while dark green indicates overlapping of model and rain gauge data. First row: ALADIN 8km, Second row: ALADIN 2km upscaled to ALADIN 8km grid.



## Figure 8

Figure 8: Mean sea level pressure (a) and 850 hPa geopotential height (blue isolines), wind speed (background shading) and direction (vectors) (b) according to the ALADIN model operational forecast on 2100 UTC 12 September 2012 (starting from the 0000 UTC analysis of the same day). □

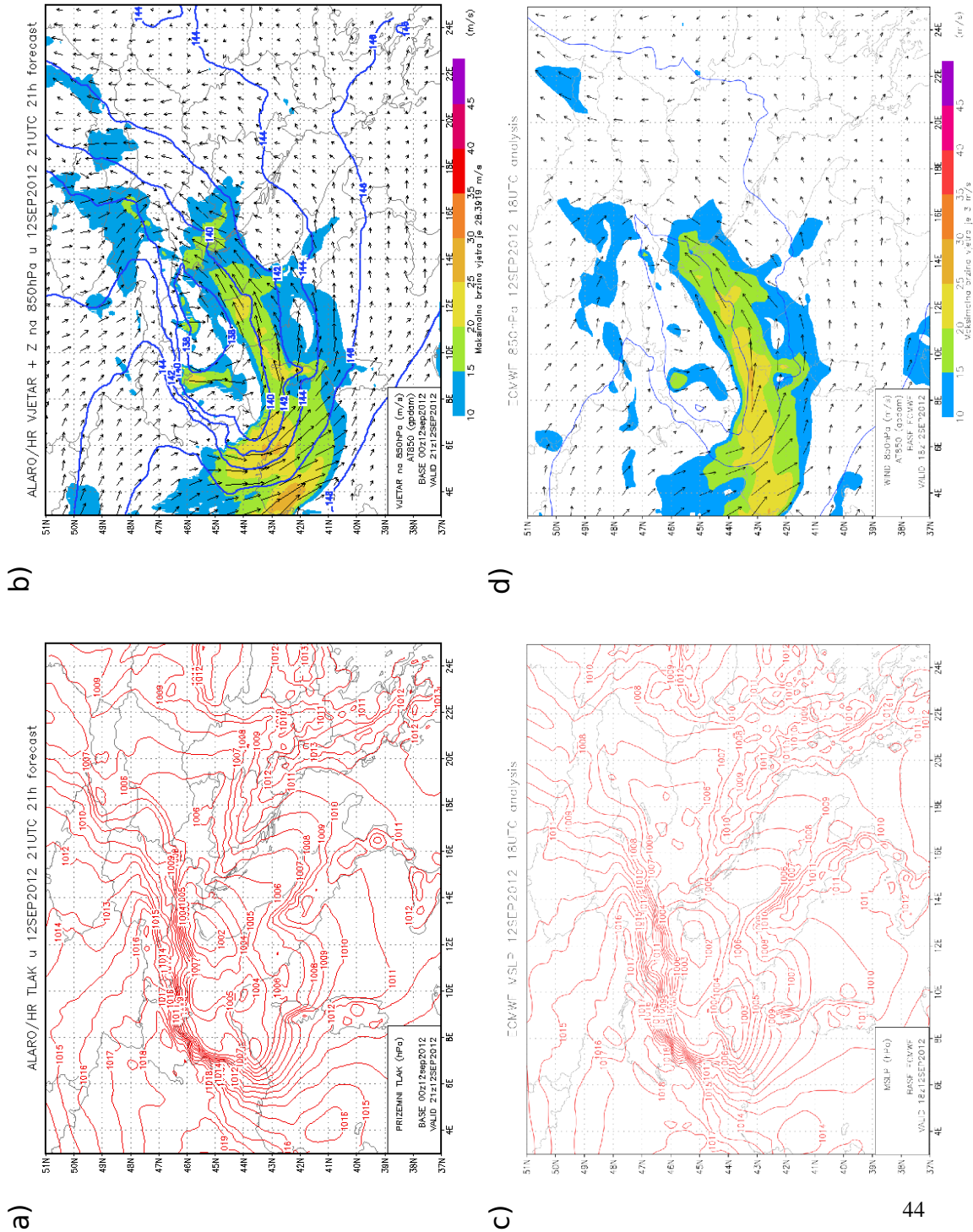




**Figure 9**

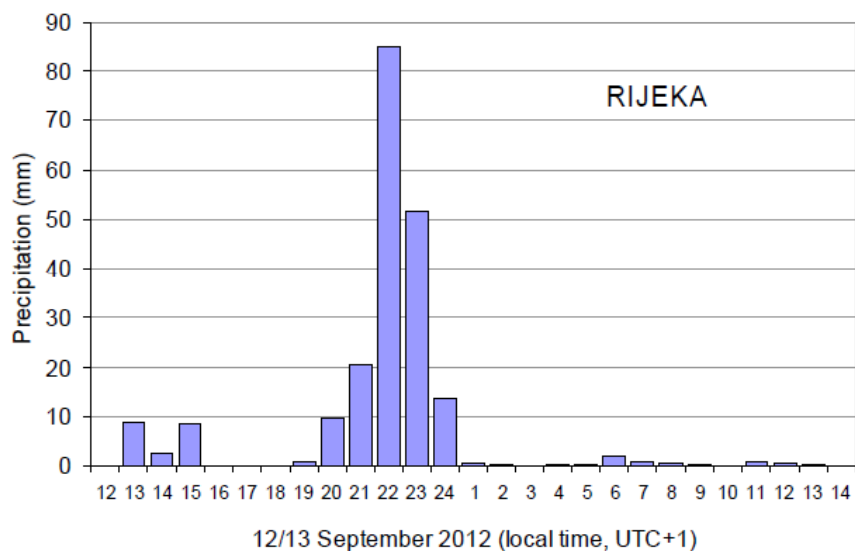


Figure 9: Hourly precipitation amounts from 1PM on 12 September 2012 to 1 PM on 13 September 2012 recorded at the Rijeka meteorological station.



Figure 10

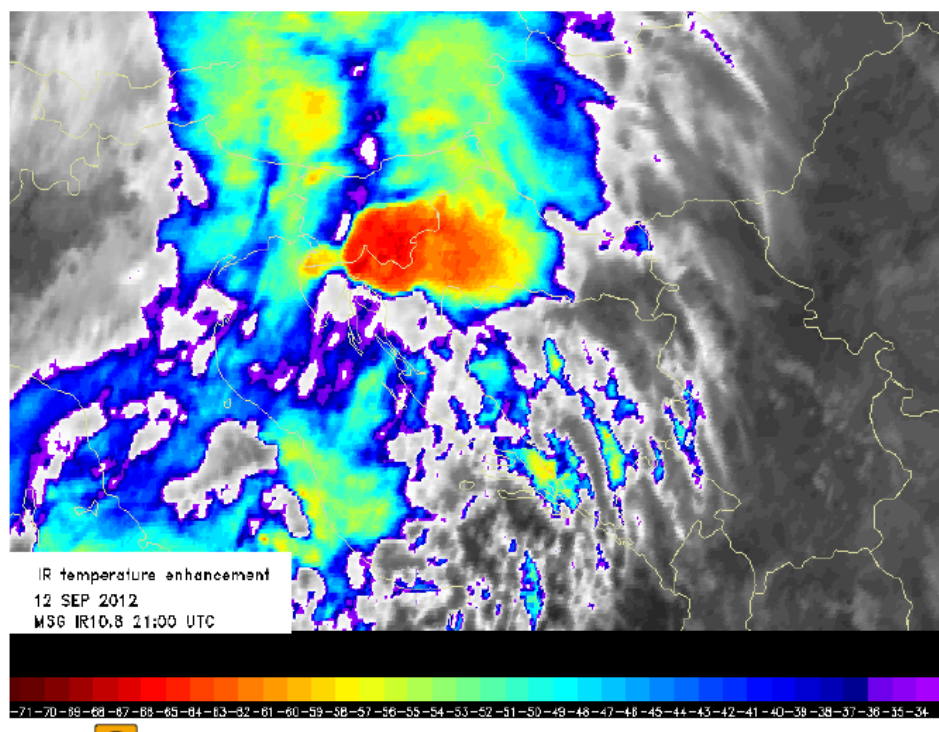


Figure 10: IR temperature enhanced satellite image for 2100 UTC on 12 September 2012 operational MSG product used in DHMZ at the time. □



Figure 11

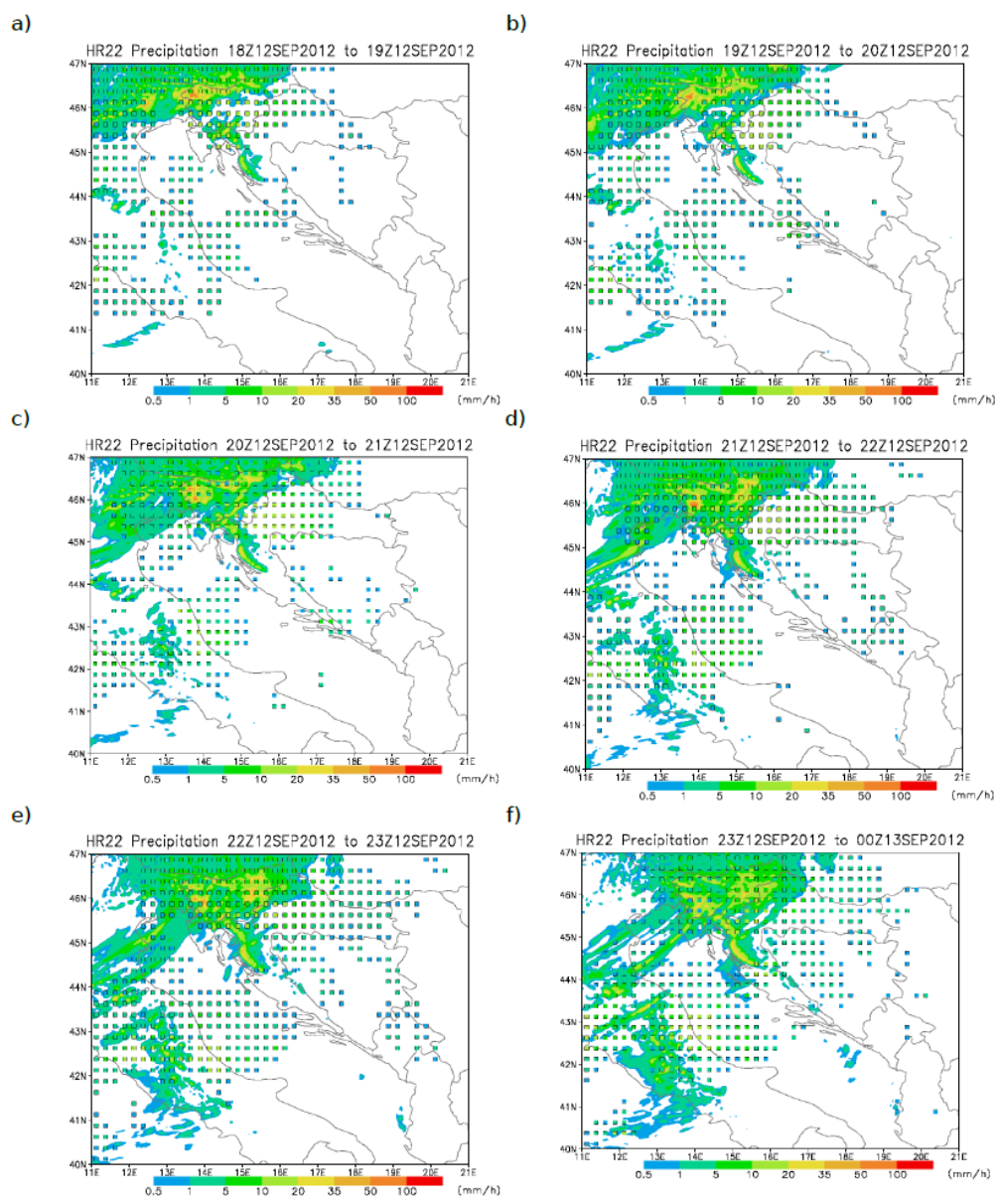


Figure 11: High resolution forecast of hourly accumulated precipitation (shaded background) and TRMM 3B41RT precipitation estimates (squares) for 1900 (a), 2000 (b), 2100 (c), 2200 (d) and 2300 (e) UTC 12 and 0000 (f) UTC 13 September 2012, this was the period of highest precipitation intensity. Satellite derived precipitation data are used as provided from the Tropical Rainfall Measuring Mission (TRMM, (Huffman et al. 2007)), in particular we used the hourly precipitation intensity data from 3B41RT product.



Figure 12

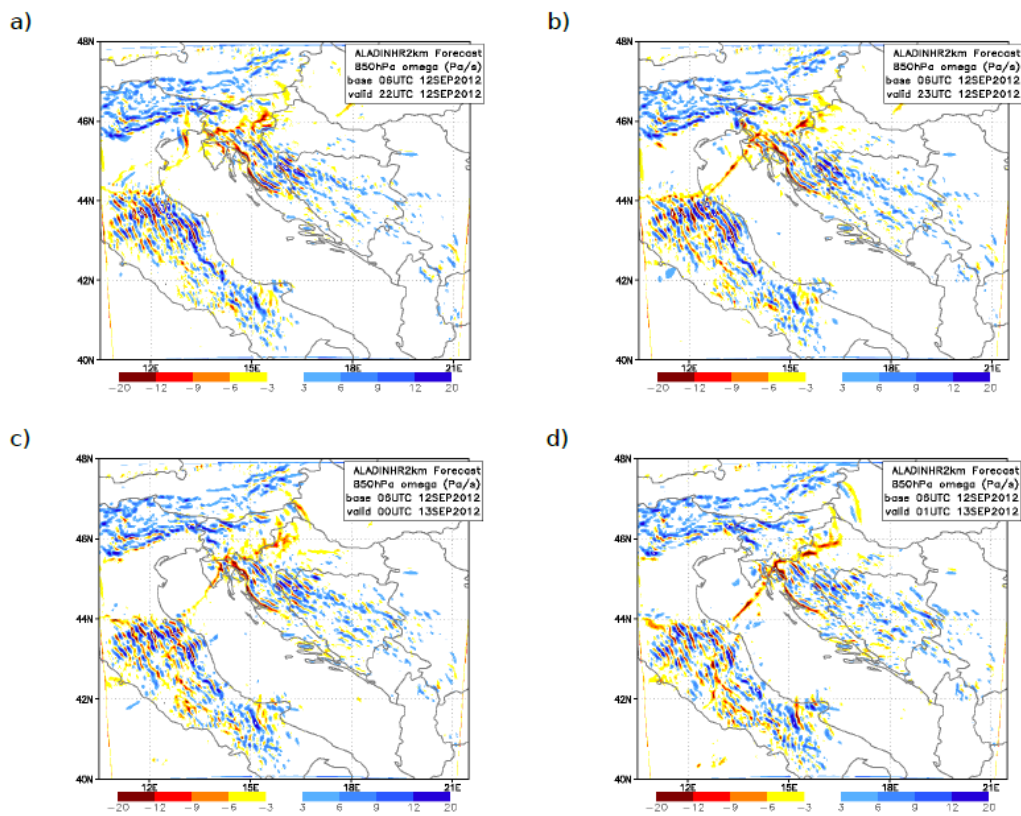


Figure 12: Vertical velocity omega (Pa/s) at 850 hPa level from the operational 2 km resolution forecast for 2200 (a) and 2300 (b) UTC on 12 and 0000 (c) and 0100 (d) UTC on 13 September 2012, upward motions are shown in shades of red and downward in blue. □



**Figure 13**

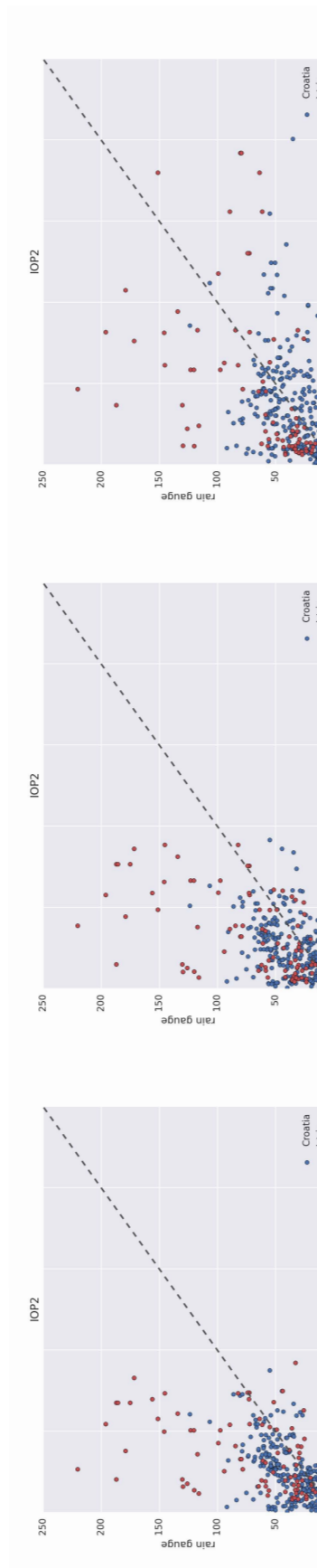


Figure 13: Scatter plot of 24h accumulated precipitation from rain gauges over Croatia and model equivalent from ALADIN 8 km (left), ALADIN 8 km without data assimilation (middle), ALADIN 2 km (right) model and from the point nearest to the location of rain gauge for IOP2. Locations from Istria peninsula are marked with red colour.



### 24h accumulated precipitation (2012-09-12 06UTC - 2012-09-13 06UTC)

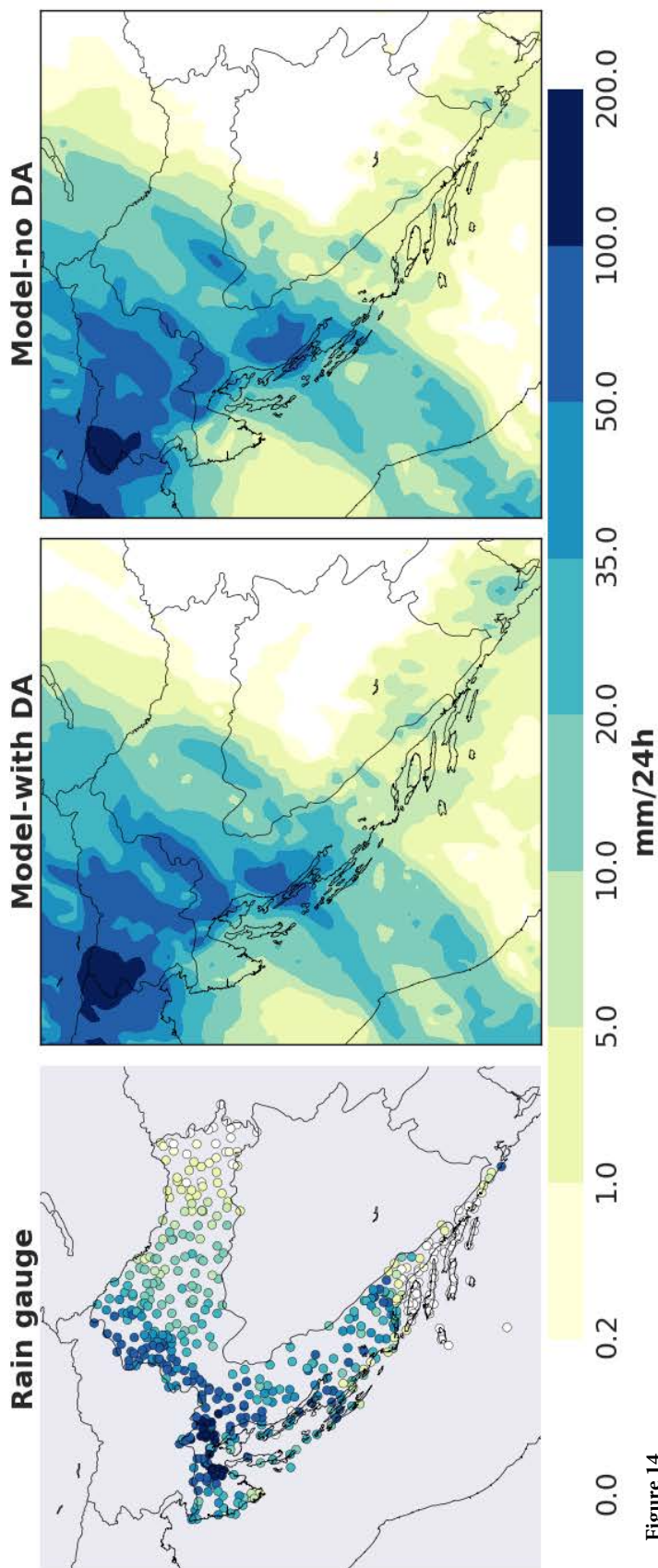


Figure 14

Figure 14: 24h accumulated precipitation from 12 Sep 0600 UTC until 13 Sep 0600 UTC (IOP12).  
Left: rain gauge measurement, middle: ALADIN 8 km operational forecast with data  
assimilation, right: ALADIN 8 km forecast without data assimilation. □